博士論文

Nanomaterials Fabrication by using Pulsed Laser Ablation with Sonochemistry in an Aqueous Environment for Composite Materials

Xin Hu

Goto Laboratory

Department of Materials Process Engineering
Graduate School of Engineering
Nagoya University

Table of Content

CHAPTER 1

Introduction

1-1 Background and outline of the Thesis

1-1-1 Nanomaterials

Nanomaterials have gotten a lot of attention as an interesting and novel class of materials with a wide variety of practical applications. The length of one nanometer could be known by lining up three calcium atoms or five sulfur atoms, which equals one nanometer. If the size of materials is in the range of 1 – 100 nm, there are classified as nanomaterials [1]. The physicochemical characteristics of nanomaterials differ from those of bulk materials, which are essentially dependent on their size and form. It is difficult to clarify the exact time of the first utilization of nanosized materials by humans. However, even in the fourteenth and thirteenth centuries BCE, the starting of glassmaking in Mesopotamia and Egypt appears to have begun. Actually, as revealed by many chemical investigations done on these historical treasures, the red color in some glasses is explained by the presence either of cuprous oxide nanoparticles or metal copper nanoparticles [2]. The application of metal nanoparticles was also found in a piece of Roman glass art, the Lycurgus Cup, which is produced in the fourth century CE and exhibited in the British Museum in London [3]. With the development of science and technology, nanomaterials have been applicated in a variety of areas, such as electronics, energy, biomedicine, environment

and food. Lee et al. [4] have reported that nano-carbon materials such as graphene and carbon nanotubes (CNTs) have a huge potential to replace silicon as a material for producing faster, smaller and more efficient microchips and electron devices because of excellent elastic properties as well as the outstanding combination of electronic and thermal property compared to conventional silicon material. Besides, in the food industry, Mustafa et al. [5] have found that nanomaterial-based sensors provide the opportunity to detect contamination in the food rapidly. Several types of nanomaterial have been utilized in the food packaging area to extend the shelf-life of foods and inhibit the growth of the bacterial [6].

Among the nanomaterials, nanoparticles (NPs) have attracted a lot of interest in recent years. The particles that range in size from 1 to 100 nanometers can be called NPs, which are almost made up of metal, carbon, metal oxides or organic substances [7]. Compared with their bulk particles at a larger size, NPs exhibit novel physical, chemical and biological properties as a result of a comparatively larger surface area to the volume, enhanced mechanical property and improved stability and reactivity in a process [8]. The unique properties of NPs have led to their application in various areas, such as medicine, affordable and clean energy, catalysis and electronics. Huo et al. [9] have investigated that gold NPs can be utilized to construct biosensors, such as immunosensors, enzyme sensors and DNA sensors, due to the excellent ability to immobilize biomolecules. In addition, as a result of the antibacterial property of silver NPs, they have been utilized to control the growth of bacterial in various areas, such as dental work, biomedical devices and tissue engineering [10]. With the continuous

research on nanomaterials, nanotechnology will gain a great future because of its huge potential to change the environment and even the lifestyle of people.

1-1-2 Laser Ablation

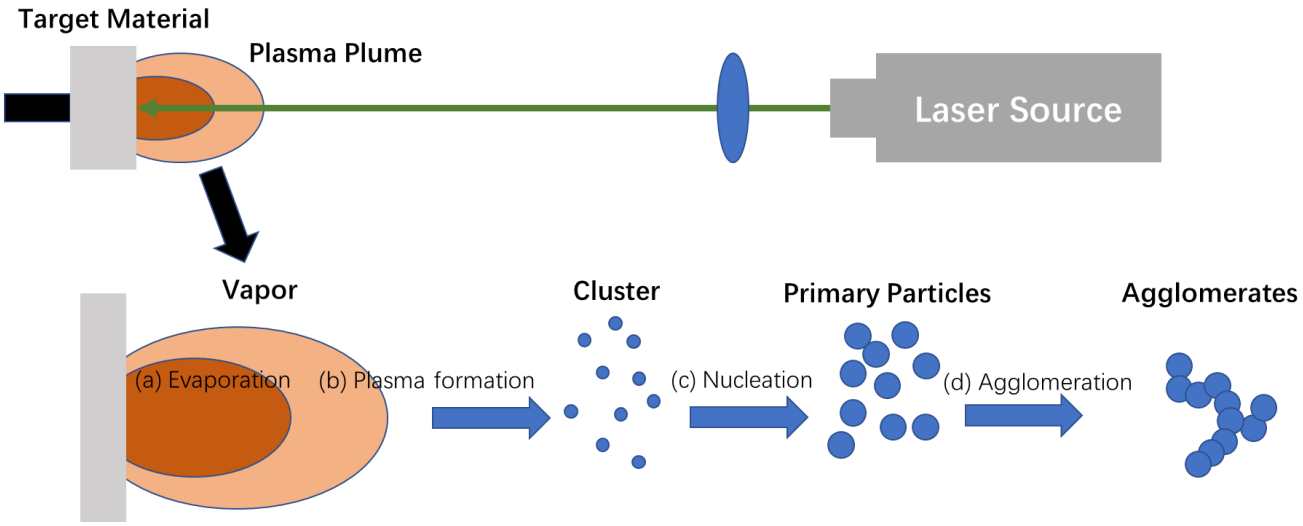

Figure 1. Schematic of particle generation in the laser ablation process.

There are plenty of manufacturing methods and tools utilized for the fabrication of nanomaterials. Each manufacturing method has benefits and drawbacks. Among these methods, laser-assisted fabrication of functional nanomaterials is unquestionably one of the most important methods. Laser, which means a very narrow beam of light, has been widely applicated in a lot of technologies and instruments since it was first invented by Theodore H. Maiman at Hughes Research Laboratories [11]. The letters in the word laser represent Light Amplification by Stimulated Emission of Radiation. Actually, laser ablation is a technique for ablating solid target materials by utilizing a laser as the energy source. In the ablation process, incredibly high energy is concentrated at a particular point on the surface of the solid to evaporate the light-

absorbing material. Not only a single photon process (breaking the chemical bonds) but also multiphoton excitation (thermal evaporation) can occur in the process of removing the atoms of the absorbing material, which generates high-purity nanoparticles [12]. Generally, the purity of the target material and surrounding environment (vacuum, gas or liquid) can determine the purity of the fabricated nanoparticles. And the size distribution, crystal structure and agglomeration of the produced nanoparticles are difficult to control due to the complex process of laser ablation [13]. **Fig. 1** shows a schematic of particle generation in the laser ablation process. The temperature of the irradiated spot rapidly rises when the laser is focused on the surface of a solid target to vaporize the target material. Collisions between evaporating species (atoms and clusters) and surrounding molecules cause light emission, electron state excitation and the production of electrons and ions, resulting in the generation of a laser-induced plasma plume [14]. The parameters in the process, such as laser parameters, the target material, ambient environment (vacuum, gas or liquid), ambient temperature and pressure, all have an impact on the property of the generated plasma plume. Garrelie et al. [15] have researched the influence of the ambient gas nature and pressure on the laser-induced plasma plume by Monte Carlo simulation and found a huge difference when utilizing different gas as the ambient media (argon and krypton atmosphere). The generated clusters aggregate into nanoparticles, which was then formed nanoparticles chains. The reason may be that the primary nanoparticles adhere to each other during the plume expansion, resulting in the generation of different structures of materials ranging from spherical particles

to line nanostructure [16].

The ambient environment can have a huge impact on the fabricated nanomaterials. Generally, since 1965, Smith et al. [17] have studied pulsed laser deposition (PLD) in the vacuum chambers to fabricate the thin film. In the process of PLD, the materials are vaporized from the target solid under the atmosphere of ultrahigh vacuum or in the presence of the background gas to generate the plasma plume, which is subsequently deposited on a substrate and changes to a thin film. This method has been successfully utilized to generate a variety of thin films with an excellent crystalline quality, such as metallic multilayers, ceramic oxides, polycrystalline as well as nitrides [18]. As for the fabrication of the thin films, compared to other methods (metal-organic chemical vapor deposition or molecular beam epitaxy), PLD has a relatively lower cost and the crystalline quality of the fabricated product is higher [19].

With the rise of nanotechnology, laser ablation (LA) has been widely utilized for the fabrication of nanoparticles. Firstly, LA is usually combined with the vacuum chamber. Amoruso et al. [20] have reported the successful generation of silicon nanoparticles with the size of 5-25 nm by LA of silicon targets in the vacuum. Nevertheless, apart from that the LA in the vacuum is an adaptable method to prepare for the nanomaterials, advantages of this method are mainly the broad size and concentration distribution of the fabricated nanoparticles [21]. LA in different ambient gases such as argon, helium and nitrogen has been utilized to improve the production rate and decrease the size of the fabricated silver nanoparticles [22]. It was found that

silver nanoparticles can be fabricated and controlled in the range of 4-20 nm by choosing the appropriate type and pressure of the gas. The mean size of silver nanoparticles increased with the increasing molecular weight of the ambient gas and decreased with increasing gas pressure. After various research on the LA in the vacuum and ambient gas, the researchers started trying to change the ambient media to the liquid. Patil et al. [23] firstly reported utilizing LA in liquid to fabricate a metastable product of iron oxide by ablating a pure iron target material in 1987. LA in liquid has been utilized to fabricate nanoparticles as a fungible chemical method since the LA in liquid is regarded as a cleaner and more simple process. The nature of the liquid media has a huge impact on the fabrication of the nanoparticles. For example, Mohammad et al. [24] have found that compared to acetone and distilled water, utilizing ethanol as the ambient media in the LA process can right in the generation of smaller nanoparticles as well as narrow size distribution. A variety of researchers have studied the fabrication of several types of nanoparticles by using LA in the distilled water [25, 26], acetone [27, 28], sodium dodecyl sulfate (SDS) [29, 30], polyvinylpyrrolidone (PVP) [31, 32], liquid nitrogen solutions (LN) [33], ethanol and ethylene chloride [34-36]. Although, the ambient media of LA process can be vacuum and gas, which has been widely developed, the advancement of the methods performed in the liquid media has been of the greatest interest to researchers. Deionized water is also the best medium for generating nanoparticles.

1-1-3 Sonochemistry

Sonochemistry, which means molecules undergo chemical reactions as a result of

the utilization of powerful ultrasonic irradiation at the frequency of 20 kHz to 10 MHz, has been widely applicated to fabricate nanomaterials [37]. The phenomenon of acoustic cavitation is responsible for the sonochemical effects in liquids. When applicating ultrasonic waves in the liquid media, it can generate a pattern of compressions and rarefactions that exert positive and negative pressure to the liquid phase. This can push or pull molecules together or away from one another in the liquid and generate plenty of bubbles. Within a few microseconds, the growth and immediate collapse of the bubbles in the liquid can generate local special hot spots with high temperatures (up to 5000 ℃) and pressures (exceeding 500 atm) [38]. In addition, the formation of shock waves and micro-jets exceeding 400 km/h also occurs [39]. The sonochemistry method has been one of the earliest techniques to fabricate nanomaterials due to its simplicity of utilization, fastness, and environmental benefits [40]. There are various nanomaterials fabricated by sonochemical synthesize, such as gold nanoparticles [41], iron nanoparticles [42], ZnO nanosized oxides [43] and so on. In addition, sonochemistry is an outstanding method for coating the surface by forming a smooth layer of the coated materials. Gnanaraj et al. [44] have successfully coated $LiMn_2O_4$ with MgO sonochemically.

1-2 Motivation and Purpose of the Present Work

This work focused on the fabrication of metal nanoparticles by utilizing pulsed laser ablation and sonochemistry. Various parameters which affect the fabricated nanoparticles have been researched to find the optimal conditions. In addition, the

fabricated nanoparticles also are further applicated as the source of composite nanomaterials.

The content is as follows. A brief introduction of nanomaterials, laser ablation and sonochemistry is given in Chapter 1. In Chapters 2 and 3, a detailed discussion about this work is given, about the fabrication of metal nanoparticles by laser ablation and sonochemical synthesize and the further application of fabricated composite nanomaterials by combining metal nanoparticles with polymers.

Reference

[1] L.A. Kolahalam, I.K. Viswanath, B.S. Diwakar, B. Govindh, V. Reddy, Y. Murthy, Review on nanomaterials: Synthesis and applications, Materials Today: Proceedings 18 (2019) 2182-2190.

[2] R.H. Brill, N.D. Cahill, A red opaque glass from Sardis and some thoughts on red opaques in general, Journal of Glass Studies (1988) 16-27.

[3] I. Freestone, N. Meeks, M. Sax, C. Higgitt, The Lycurgus cup—a roman nanotechnology, Gold bulletin 40(4) (2007) 270-277.

[4] S.H. Chae, Y.H. Lee, Carbon nanotubes and graphene towards soft electronics, Nano Convergence 1(1) (2014) 1-26.

[5] F. Mustafa, R.Y. Hassan, S. Andreescu, Multifunctional nanotechnology-enabled sensors for rapid capture and detection of pathogens, Sensors 17(9) (2017) 2121.

[6] P. Chaudhary, F. Fatima, A. Kumar, Relevance of nanomaterials in food packaging and its advanced future prospects, Journal of inorganic and

organometallic polymers and materials 30(12) (2020) 5180-5192.

[7] S. Hasan, A review on nanoparticles: their synthesis and types, Res. J. Recent Sci 2277 (2015) 2502.

[8] M. Hassellöv, J.W. Readman, J.F. Ranville, K. Tiede, Nanoparticle analysis and characterization methodologies in environmental risk assessment of engineered nanoparticles, Ecotoxicology 17(5) (2008) 344-361.

[9] Q. Huo, A perspective on bioconjugated nanoparticles and quantum dots, Colloids and Surfaces B: Biointerfaces 59(1) (2007) 1-10.

[10] X.-F. Zhang, Z.-G. Liu, W. Shen, S. Gurunathan, Silver nanoparticles: synthesis, characterization, properties, applications, and therapeutic approaches, International journal of molecular sciences 17(9) (2016) 1534.

[11] C.H. Townes, Birth of the maser and laser, Optical Chemical Sensors, Springer2006, pp. 1-15.

[12] M. Kim, S. Osone, T. Kim, H. Higashi, T. Seto, Synthesis of nanoparticles by laser ablation: A review, KONA Powder Part. J. (2017) 2017009.

[13] H. Zeng, X.W. Du, S.C. Singh, S.A. Kulinich, S. Yang, J. He, W. Cai, Nanomaterials via laser ablation/irradiation in liquid: a review, Advanced Functional Materials 22(7) (2012) 1333-1353.

[14] G.W. Yang, Laser ablation in liquids: Applications in the synthesis of nanocrystals, Progress in Materials Science 52(4) (2007) 648-698.

[15] F. Garrelie, C. Champeaux, A. Catherinot, Expansion dynamics of the plasma plume created by laser ablation in a background gas, Applied Physics A

69(1) (1999) S55-S58.

[16] O.R. Musaev, E.A. Sutter, J.M. Wrobel, M.B. Kruger, Au, Ge, and AuGe nanoparticles fabricated by laser ablation, Journal of Nanoparticle Research 14(2) (2012) 654.

[17] H.M. Smith, A. Turner, Vacuum deposited thin films using a ruby laser, Applied Optics 4(1) (1965) 147-148.

[18] D.B. Chrisey, G.K. Hubler, Pulsed laser deposition of thin films, (1994).

[19] D. Johnson, Y. Chen, Y. He, R. Prince, Deposition of carbon nitride via hot filament assisted CVD and pulsed laser deposition, Diamond and related materials 6(12) (1997) 1799-1805.

[20] S. Amoruso, R. Bruzzese, N. Spinelli, R. Velotta, M. Vitiello, X. Wang, G. Ausanio, V. Iannotti, L. Lanotte, Generation of silicon nanoparticles via femtosecond laser ablation in vacuum, Applied Physics Letters 84(22) (2004) 4502-4504.

[21] P. Willmott, J. Huber, Pulsed laser vaporization and deposition, Reviews of Modern Physics 72(1) (2000) 315.

[22] W.T. Nichols, G. Malyavanatham, D.E. Henneke, J.R. Brock, M.F. Becker, J.W. Keto, H.D. Glicksman, Gas and pressure dependence for the mean size of nanoparticles produced by laser ablation of flowing aerosols, Journal of Nanoparticle Research 2(2) (2000) 141-145.

[23] P. Patil, D. Phase, S. Kulkarni, S. Ghaisas, S. Kulkarni, S. Kanetkar, S. Ogale, V. Bhide, Pulsed-laser–induced reactive quenching at liquid-solid

interface: Aqueous oxidation of iron, Physical review letters 58(3) (1987) 238.

[24] M.H. Mahdieh, B. Fattahi, Size properties of colloidal nanoparticles produced by nanosecond pulsed laser ablation and studying the effects of liquid medium and laser fluence, Applied Surface Science 329 (2015) 47-57.

[25] M. Boutinguiza, M. Meixus, J. Del Val, A. Riveiro, R. Comesaña, F. Lusquiños, J. Pou, Synthesis and characterization of Pd nanoparticles by laser ablation in water using nanosecond laser, Physics Procedia 83 (2016) 36-45.

[26] K.S. Khashan, F.A. Abdulameer, M.S. Jabir, A.A. Hadi, G.M. Sulaiman, Anticancer activity and toxicity of carbon nanoparticles produced by pulsed laser ablation of graphite in water, Advances in Natural Sciences: Nanoscience and Nanotechnology 11(3) (2020) 035010.

[27] N. Tarasenko, A. Butsen, E. Nevar, Laser-induced modification of metal nanoparticles formed by laser ablation technique in liquids, Applied surface science 247(1-4) (2005) 418-422.

[28] A. Menendez-Manjon, J. Jakobi, K. Schwabe, J.K. Krauss, S. Barcikowski, Mobility of nanoparticles generated by femtosecond laser ablation in liquids and its application to surface patterning, JLMN-Journal of Laser Micro/Nanoengineering 4(2) (2009) 95-99.

[29] C. Liang, Y. Shimizu, T. Sasaki, N. Koshizaki, Preparation of ultrafine TiO 2 nanocrystals via pulsed-laser ablation of titanium metal in surfactant solution, Applied physics A 80(4) (2005) 819-822.

[30] F. Mafuné, J.-y. Kohno, Y. Takeda, T. Kondow, H. Sawabe, Structure and

stability of silver nanoparticles in aqueous solution produced by laser ablation, The Journal of Physical Chemistry B 104(35) (2000) 8333-8337.

[31] T. Tsuji, D.-H. Thang, Y. Okazaki, M. Nakanishi, Y. Tsuboi, M. Tsuji, Preparation of silver nanoparticles by laser ablation in polyvinylpyrrolidone solutions, Applied Surface Science 254(16) (2008) 5224-5230.

[32] T. Tsuji, T. Mizuki, S. Ozono, M. Tsuji, Laser-induced silver nanocrystal formation in polyvinylpyrrolidone solutions, Journal of Photochemistry and Photobiology A: Chemistry 206(2-3) (2009) 134-139.

[33] K. Sasaki, N. Takada, Liquid-phase laser ablation, Pure and Applied Chemistry 82(6) (2010) 1317-1327.

[34] S. Dolgaev, A. Simakin, V. Voronov, G.A. Shafeev, F. Bozon-Verduraz, Nanoparticles produced by laser ablation of solids in liquid environment, Applied surface science 186(1-4) (2002) 546-551.

[35] T. Ohshima, S. Nakashima, T. Ueda, H. Kawasaki, Y. Suda, K. Ebihara, Laser ablated plasma plume characteristics for photocatalyst TiO2 thin films preparation, Thin Solid Films 506 (2006) 106-110.

[36] R. Ganeev, M. Baba, A. Ryasnyansky, M. Suzuki, H. Kuroda, Characterization of optical and nonlinear optical properties of silver nanoparticles prepared by laser ablation in various liquids, Optics Communications 240(4-6) (2004) 437-448.

[37] K.S. Suslick, S.-B. Choe, A.A. Cichowlas, M.W. Grinstaff, Sonochemical synthesis of amorphous iron, nature 353(6343) (1991) 414-416.

[38] R. Feng, Y. Zhao, C. Zhu, T. Mason, Enhancement of ultrasonic cavitation yield by multi-frequency sonication, Ultrasonics sonochemistry 9(5) (2002) 231-236.

[39] A. Shui, W. Zhu, L. Xu, D. Qin, Y. Wang, Green sonochemical synthesis of cupric and cuprous oxides nanoparticles and their optical properties, Ceramics International 39(8) (2013) 8715-8722.

[40] J.H. Bang, K.S. Suslick, Applications of ultrasound to the synthesis of nanostructured materials, Adv. Mater. 22(10) (2010) 1039-1059.

[41] X.-F. Qiu, J.-J. Zhu, H.-Y. Chen, Controllable synthesis of nanocrystalline gold assembled whiskery structures via sonochemical route, Journal of crystal growth 257(3-4) (2003) 378-383.

[42] Y. Yu, Q. Zhang, X. Li, Reduction process of transition metal ions by zinc powder to prepare transition metal nanopowder, Acta Physico-Chimica Sinica 19(5) (2003) 436-440.

[43] D. Qian, J. Jiang, P.L. Hansen, Preparation of ZnO nanocrystals via ultrasonic irradiation, Chemical communications (9) (2003) 1078-1079.

[44] J. Gnanaraj, V. Pol, A. Gedanken, D. Aurbach, Improving the high-temperature performance of LiMn2O4 spinel electrodes by coating the active mass with MgO via a sonochemical method, Electrochemistry Communications 5(11) (2003) 940-945.

CHAPTER 2

Ultrasonic-Enhanced Fabrication of Metal Nanoparticles by Laser Ablation in Liquid

2-1 Introduction

Nanoparticles with sizes of 1–100 nm have specific and superior physical and chemical properties compared to their bulk materials owing to their large surface area and quantum size effect [1]. They have been widely utilized in many areas such as photochemistry, catalysis, and biomedicine. Recently, significant attention has been focused on gold (AuNPs) and silver (AgNPs) nanoparticles due to their unique properties. The versatility of AuNPs has offered valuable materials for a variety of applications. In diagnostics, AuNPs are able to bind with analytes, resulting in modification of the physicochemical properties of gold nanoparticles such as surface plasmon resonance, redox behavior, and conductivity, which could be detected as signals [2]. The large surface area for loading drugs, nontoxicity, and stability also make them functional in drug delivery systems [3]. With regard to AgNPs, they have been utilized as anti-bacterial agents in the health market, for food storage, and in water treatment, in addition to many environmental applications [4].

Various approaches have been reported for synthesizing metal nanoparticles, such as the seeding growth method, arc discharge plasma, and chemical vapor deposition (CVD). Ziegler et al. [5] presented a seeded growth approach to fabricating gold nanoparticles with diameters of 15–300 nm. The procedure for growing seeds was

mixing a precursor solution containing $H[AuCl_4] \cdot 3H_2O$ with a reducing solution containing trisodium citrate and ascorbic acid, under stirring over a period of about 45 min. The mixture was maintained at boiling temperature for about 30 min. As the ascorbic acid and sodium citrate played the roles of reducing and stabilizing agents, respectively, the fabricated AuNPs showed good shape, uniformity, and long-term stability. Ashkarran et al. [6] introduced a one-step method to prepare colloidal silver nanoparticles using arc discharge between titanium electrodes in $AgNO_3$ solution. In their work, two titanium electrodes applied with a 15 A current were placed in the $AgNO_3$ solution. As the plasma zone was formed by arc discharge between the titanium electrodes, colloidal silver nanoparticles were prepared by reducing the $AgNO_3$ in solution. Compared with the above methods, laser ablation in liquid (LAL) is a chemically simple and environmentally friendly process with no need for extreme temperature or pressure [7]. Due to its simple process and operability, pulsed laser ablation (PLA) has attracted intense attention since ruby lasers were utilized to ablate materials in the early 1960s, owing to its vast potential in nanomaterial fabrication, micromachining, and surface cleaning. The properties of fabricated nanoparticles have a significant relationship with the ambient environment in the process of laser ablation. Compared with a vacuum or gaseous ambient, the interaction between a laser pulse and a solid target in a confining liquid environment is more complicated [8].

It is well known that ultrasound is a type of mechanical sound wave with frequencies higher than those detected by human hearing (>20 kHz). One of the most important phenomena of ultrasound is acoustic cavitation, which is the growth and

collapse of microbubbles under the effect of an ultrasonic field in a liquid. When the bubbles grow and reach a critical size, they collapse, resulting in extreme temperature conditions and various secondary effects such as light emission, surface erosion, and free radicals [9]. There are multiple applications of cavitation. For example, Takahashi et al. [10] utilized ultrasonic cavitation erosion in metalworking and surface treatment, aiming to increase the fatigue limit.

Ultrasonic-assisted fabrication of nanomaterials by LAL has already been investigated. Sasaki et al. [11] found that ultrasound can improve the production rate and crystallinity of synthesized Au and ZnO nanoparticles due to the cavitation bubbles. However, research on the craters formed on the metal plates through ultrasonic-assisted LAL has scarcely been investigated to date. In addition, the determination of the colloidal nanoparticle solution concentration is arduous due to the lower number of nanoparticles. In general, inductively coupled plasma mass spectrometry (ICP-MS) is the most precise method to determine the concentration of nanoparticles in PPM (parts per million) with a wide dynamic range from ppt (ng L^{-1}) up to levels of a few hundred ppm (mg L^{-1}). Nonetheless, this method requires a clean-room environment, high operating costs, and expensive facilities [12]. In this work, LAL was combined with ultrasound to fabricate AuNPs and AgNPs. We noticed that ultrasound not only enhances the fabrication rate but also decreases the size of nanoparticles. The craters on the silver plates formed by the LAL were also studied to compare the outcomes in the presence and absence of the ultrasonic field. Here we also provided a novel method to estimate the concentration of the fabricated colloidal

solution with low cost and adequate accuracy. Furthermore, the optical characteristics of the plasma plume during the LAL process were investigated.

2-2 Experimental Procedures

2-2-1 Materials

High-purity (99.99 %) gold and silver plates with 1 mm thickness and areas of 10 mm × 10 mm, purchased from Nilaco Co., Japan, were employed as metal targets.

2-2-2 Experimental Setup and Methods

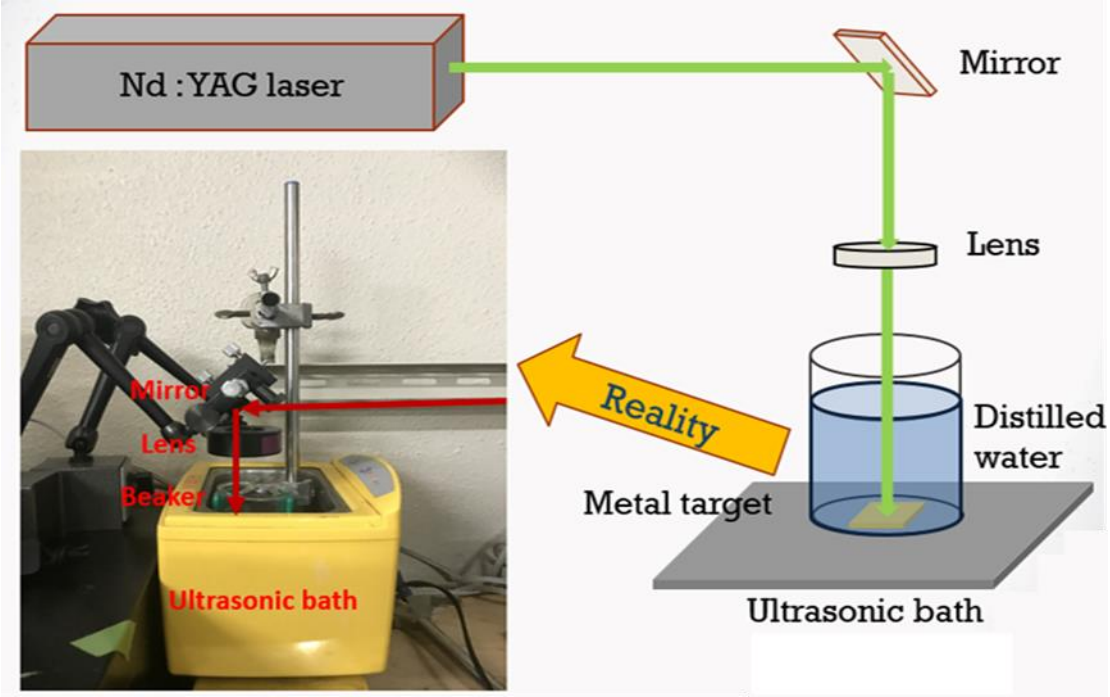

Figure 1. Schematic diagram of the ultrasonic-assisted PLA system.

A schematic of the ultrasonic-assisted PLA system for fabricating metal nanoparticles is shown in **Fig. 1.** A pulsed laser beam produced by a high-power Q-switched pulsed neodymium-doped yttrium aluminum garnet (Nd:YAG) laser (Spectra-Physics Quanta-Ray INDI-40-10), with a wavelength of 532 nm, pulse rate of 10 Hz, and pulse duration of approximately 8 ns, was utilized to ablate the metal

target, which was placed in a 50 ml glass Pyrex beaker (IWAKI TE-32, ASAHI GLASS) with 20 ml distilled water. Afterwards, the beaker container was placed inside an ultrasonic bath (ASU-2, AS ONE Company, Japan) operating at a frequency of approximately 42 kHz. The ablation times with and without applied ultrasound were 10, 20, and 40 min. The laser energy density was 26.3 J cm^{-2}.

2-2-3 Characterization of the Particles

An ultraviolet–visible (UV–vis) spectrometer (V-550, Jasco Corporation, Japan) was used to examine the optical properties of the nanoparticle colloidal solution. To analyze the morphology and elemental spectrum of the fabricated nanoparticles, a drop of nanoparticle solution was deposited on a copper grid and then analyzed by a transmission electron microscope (TEM) (JEM-2100Plus, Japan Electronic Co., Ltd) with energy-dispersive X-ray spectroscopy (EDS) (JEOL, JED-2300T & Gatan, GIF Quantum ER). The nanoparticle colloidal solutions fabricated in both the presence and absence of an ultrasonic field were loaded into a capillary cell for recording the zeta potential to check the stability by a Zetasizer Nano ZS instrument (LA-920, Malvern Instruments, Oray, France).

2-2-4 Characterization of the Craters and Concentration

The craters on the surface of the silver plate were analyzed by a scanning electron microscope (SEM) (S–4300, Hitachi, Japan) and laser microscope (LSM5PASCAL, Carl Zeiss, Germany) to obtain their morphology and three-dimensional (3D) data, which were then modeled by MATLAB to calculate the volume of the craters. By this

novel method, the concentration of the nanoparticle solution could be obtained with further application.

2-2-5 Optical Emission Spectra of the Ablation Process

To observe the differences between the presence and absence of an ultrasonic field in the LAL process, optical emission spectra were obtained using a high-resolution spectrometer (HR4000, Ocean Optics Inc.)

2-3 Results and Discussion

AuNPs and AgNPs possess optical properties (dependent upon their diameter, shape, agglomeration state, and surface structure) that are referred to as localized surface plasmon resonance (LSPR). This is a phenomenon of mutual oscillation of electrons in the conduction band of AuNPs and AgNPs resonating with a specific wavelength of the incident light. **Fig.2** shows UV spectra of the gold and silver colloidal solutions. It is observed that an intense peak of AuNPs occurs at around 520 nm, whereas the AgNPs show a sharp peak at around 405 nm. The absorption spectra are essentially in agreement with those of chemically prepared AuNPs [13] and AgNPs [14]. Spectra were taken for different ablation times (10, 20, and 40 min) in the presence and absence of the ultrasonic bath. It can be seen that the absorbance of the fabricated metal nanoparticle solution increased with the ablation time. The spectrum taken at similar ablation time revealed an increase in intensity due to the presence of the ultrasonic field. In other words, the intensity of the synthesized nanoparticle solution in the presence of an ultrasonic field is higher than that without

on the field, which implies that ultrasound can enhance the formation rate of nanoparticles in the LAL process [11, 15]. In the presence of the applied ultrasonic field, the peak at around 250 nm corresponding to the low level of free gold or silver ions in the nanoparticle suspension [16, 17] is higher than in the case without the ultrasonic field. This means that ultrasound can also improve the production rate of metal nanoparticles in the colloidal solution. The mechanism of the physical phenomenon occurring in the LAL process combined with ultrasound, which increases the nanoparticle density of the colloidal solution may be connected with the condition of the plasma plume, which were discussed in the optical emission paragraph. Furthermore, it can be seen from **Fig. 2** that the spectrum peak of ultrasound shows a little blue shift, which means smaller nanoparticles have been fabricated with ultrasound. However, the morphology and size of the fabricated AuNPs and AgNPs should be confirmed by other methods.

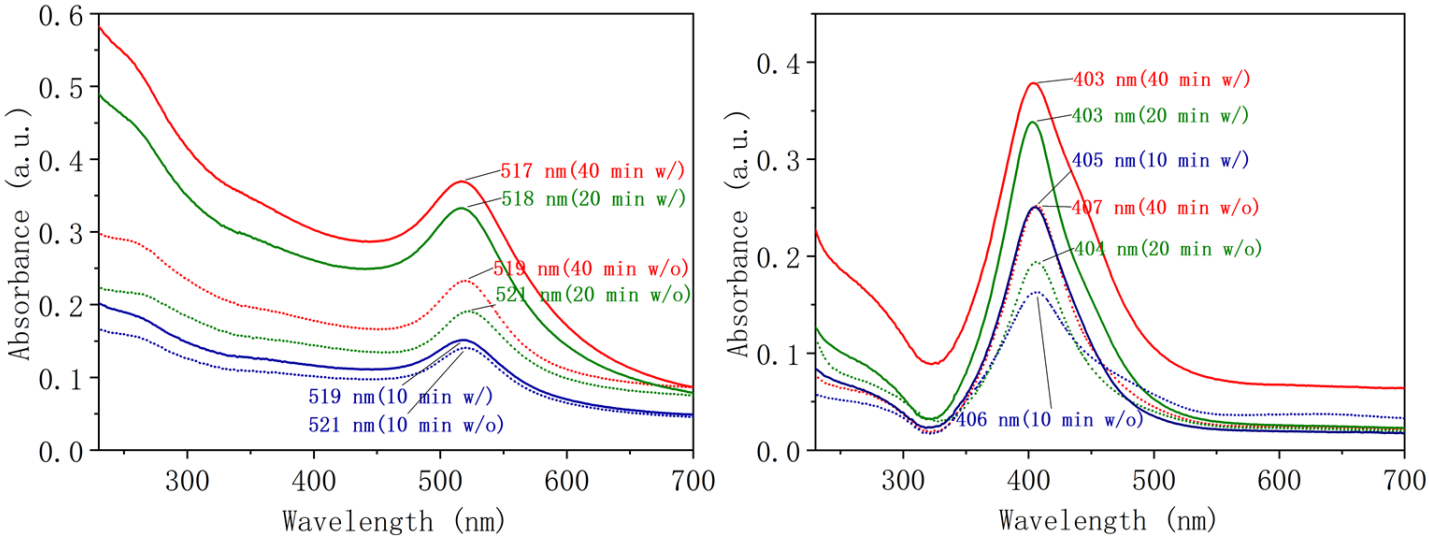

Figure 2. Optical absorbance of colloidal solutions of AuNPs (a) and AgNPs (b) with (w/) and without (w/o) an ultrasonic field for different ablation times 10, 20, and 40 min.

Fig. 3 presents TEM images of fabricated AuNPs in the presence and absence of an ultrasonic field for different ablation times. As can be seen from the diagram, the AuNPs fabricated with ultrasound are separated from each other and have spherical morphology. In contrast, in the situation without the ultrasonic field, the nanoparticles are connected with each other and have almost no clear boundary. Especially when the ablation time is 20 and 40 min, nano-networks consisting of spherical particles and wires connected with each other were respectively found. In addition, it can be seen that the nanoparticles fabricated with ultrasound are smaller than those produced without ultrasound. This result is also the same for AgNPs, as shown in **Fig. 4**, which confirms the effectiveness of ultrasound. Self-evidently, smaller nanoparticles have a higher surface-area-to-volume ratio, which is one of the reasons for some of their better properties. Raffi et al. [18] found that a larger surface-area-to-volume ratio of AgNPs provides more efficient means for enhanced antibacterial activity. From the above result, we can see that ultrasound has considerable potential in the synthesis of smaller nanoparticles in the process of LAL. The chain-like morphology of metal nanoparticle structures fabricated by LAL in distilled water has been observed by many researchers [19, 20]. During the ablation process, the nanoparticles are ejected and condensed from the high-temperature and high-pressure plasma plume formed by high-energy pulsed laser irradiation [21]. The formation of chains can be explained by the primary nanoparticles adhering to each other during plume expansion, which can form different type of nanoparticles ranging from spherical particles to line-style nanostructure [22]. Ultrasound could increase the kinetic energy and accelerate the

irregular motion of particles due to shockwaves and microjets from the local high pressure formed by the cavitation collapse in the liquid, and weaken the adhesion phenomenon between nanoparticles [23]. Smaller and more separated nanoparticles could be obtained in the presence of an ultrasonic field, as the fabrication process of nanoparticles is spatially limited and temporally shortened by the addition of the

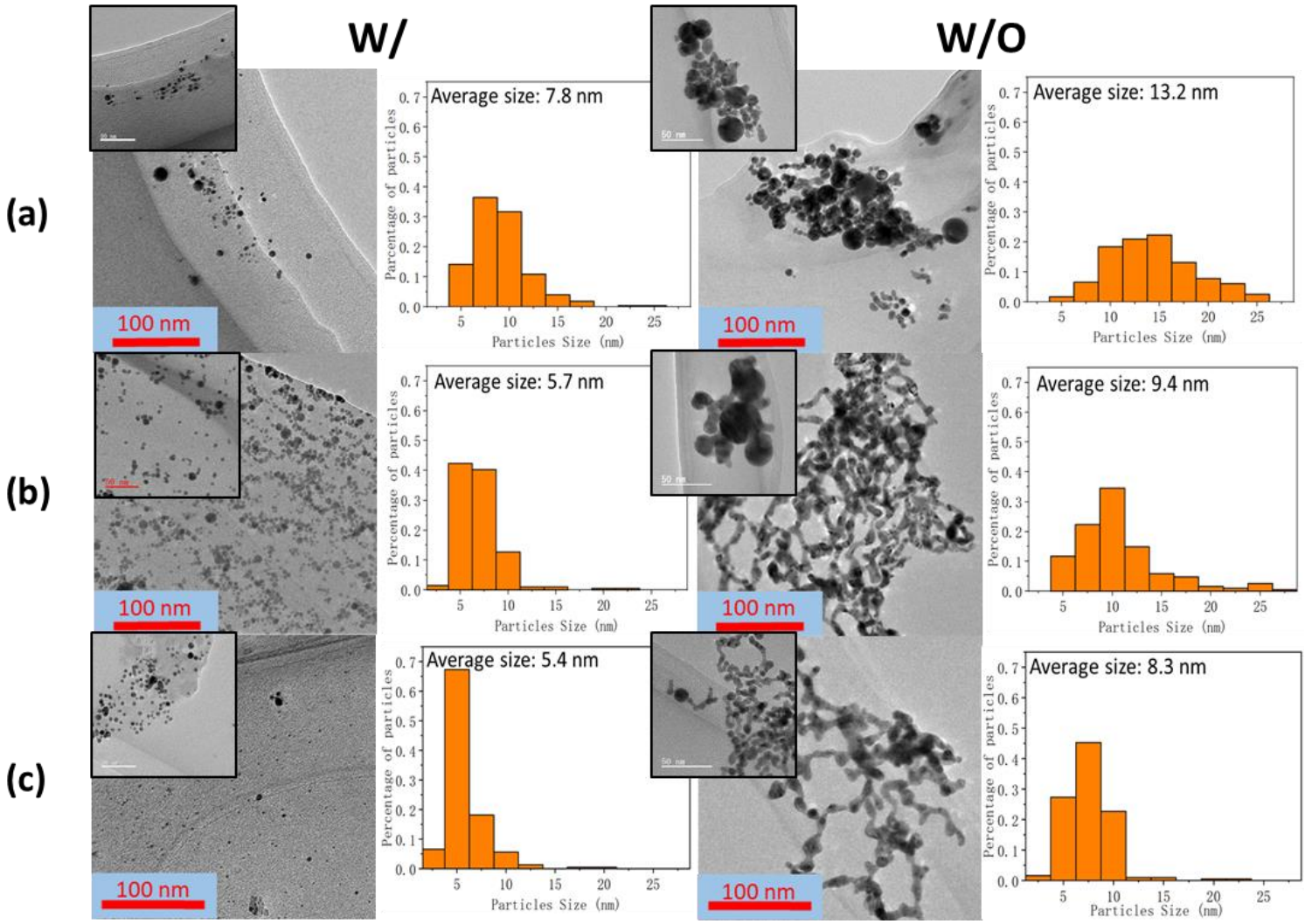

Figure 3. TEM images of AuNPs obtained when the ablation is with (w/) and without (w/o) an ultrasonic field for different ablation times 10 (a), 20 (b), and 40 (c) min.

ultrasonic pressure. Moreover, the size of the fabricated nanoparticles decreased with ablation time. Baladi et al. [24] obtained the same result by utilizing a Nd:YAG laser

to irradiate an alumina plate with different ablation times. They also found that the nanoparticle size notably decreased by extending the ablation time. This is primarily because synthesized nanoparticles that were in the laser path may have been decomposed by the high laser energy as a result of the fragmentation mechanism.

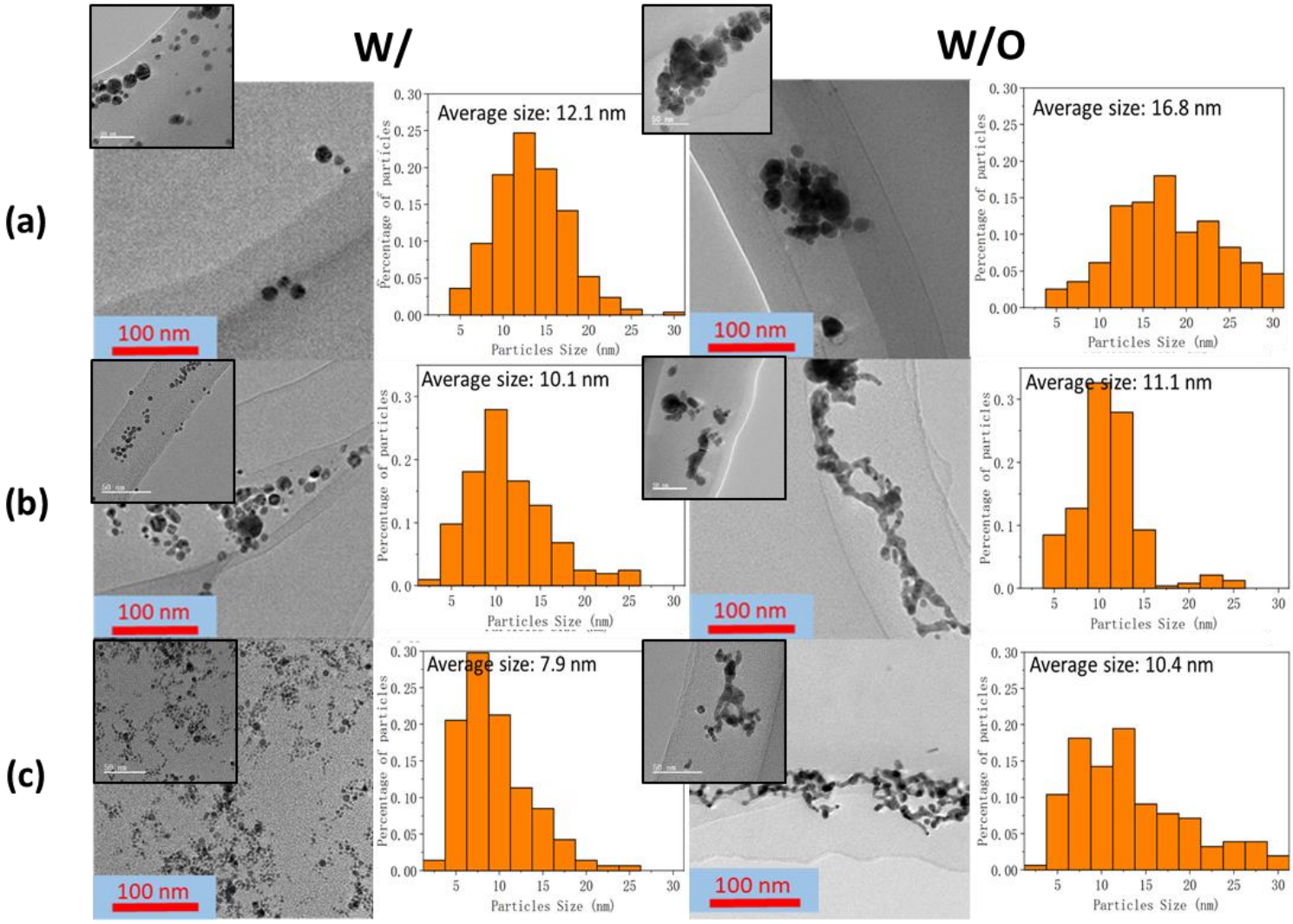

Figure 4. TEM images of AgNPs obtained when the ablation is with (w/) and without (w/o) an ultrasonic field for different ablation times 10 (a), 20 (b), and 40 (c) min.

Fig. 5 shows the high-resolution TEM (HRTEM) results of fabricated AuNPs and AgNPs in the presence and absence of an ultrasonic field when the ablation time is 20 min. The corresponding fast Fourier transform (FFT) patterns of AuNPs and AgNPs can be clearly seen from these images. In the presence of the ultrasonic field, all the

AuNPs are well crystalline with almost no structural defects. The lattice fringe spacing indicated in the image is 0.234 nm, which corresponds to the (111) facet of the crystal plane of the gold cubic phase [25]. However, in the absence of the ultrasonic field, the nanoparticles show multiple crystal planes due to the connection and overlapping between the particles. The results for the AgNPs are almost same as those of the AuNPs. The lattice fringe spacing is 0.2235 nm, corresponding to the (111) facet of the AgNPs [26].

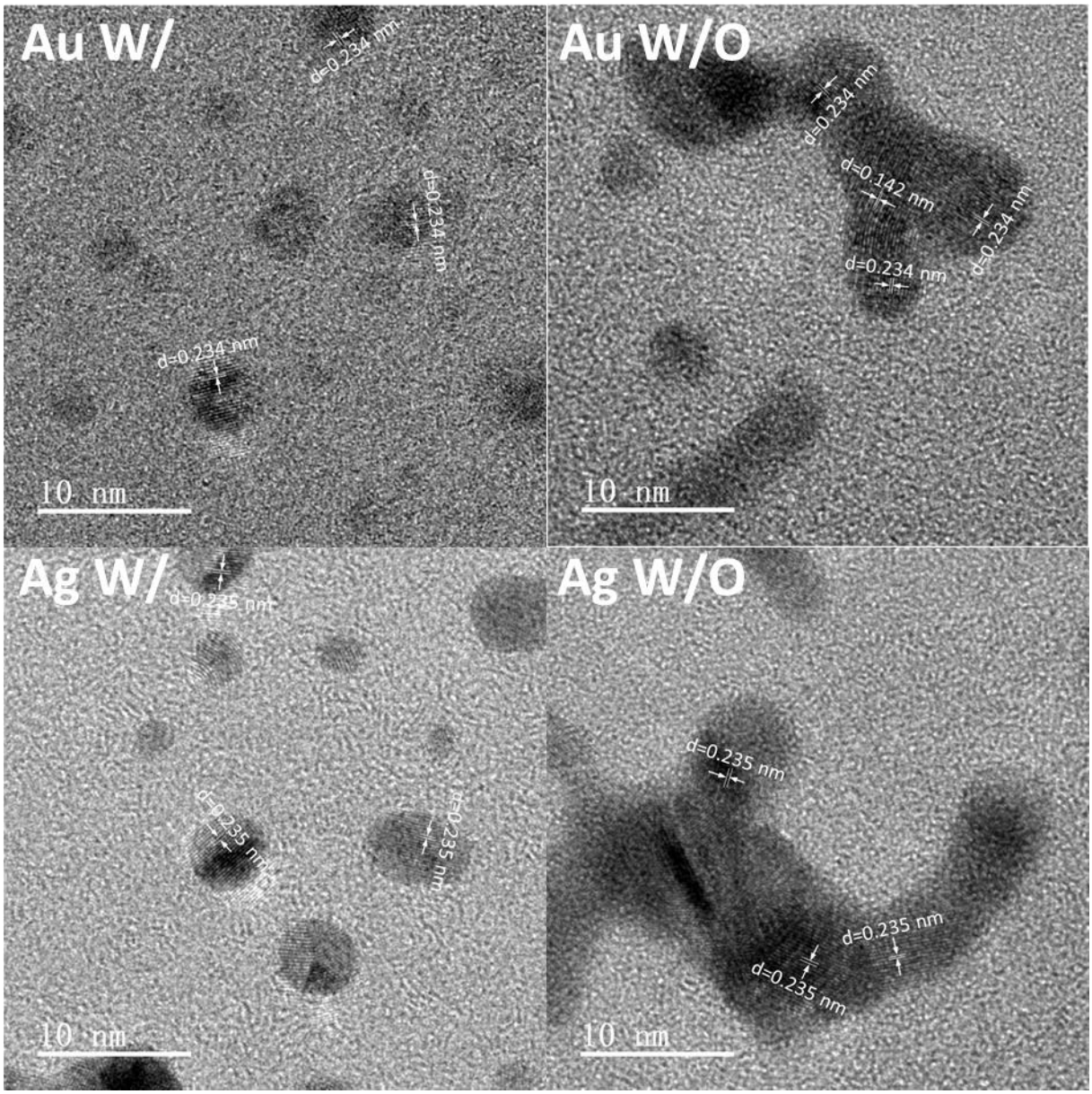

Figure 5. HRTEM images of AuNPs and AgNPs in the presence (w/) and absence (w/o) of an ultrasonic field when the ablation time is 20 min.

Fig. 6 provides the electron diffraction pattern of fabricated AuNPs in the presence (**Fig. 6a**) and absence (**Fig. 6b**) of the ultrasonic field, revealing the cubic structure of the gold. One can see that the diffraction rings of AuNPs were indexed to the (111), (200), (220), and (311) diffraction planes [27]. **Fig. 6c** and **Fig. 6d** provide the electron diffraction patterns of synthesized Agnosy in the situations with and without the ultrasonic field, respectively. No apparent differences were found by adding the ultrasonic field, which means ultrasound had no significant impact on the

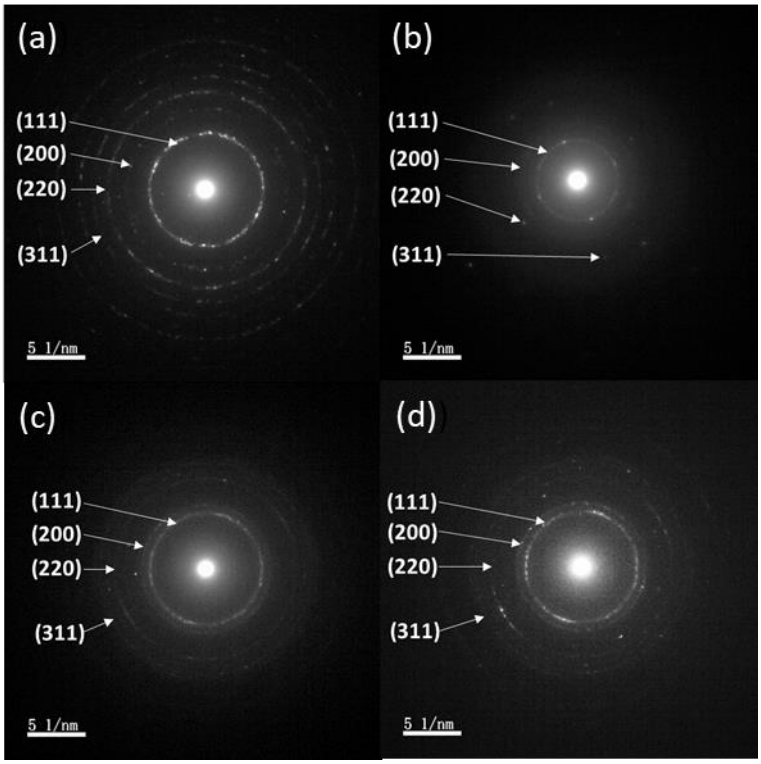

Figure 6. Selected area electron diffraction pattern of AuNPs in the presence (a) and absence (b) of an ultrasonic field, and AgNPs in the presence (c) and absence (d) of an ultrasonic field, with 20 min ablation time.

crystallinity of the fabricated nanoparticles.

Fig. 7 shows the EDS spectra of synthesized AuNPs in the presence (**Fig. 7a**) and absence (**Fig. 7b**) of an ultrasonic field. Peaks corresponding to gold, copper, oxygen, carbon, and nitrogen are clearly found in the EDS spectrum. There are not apparent

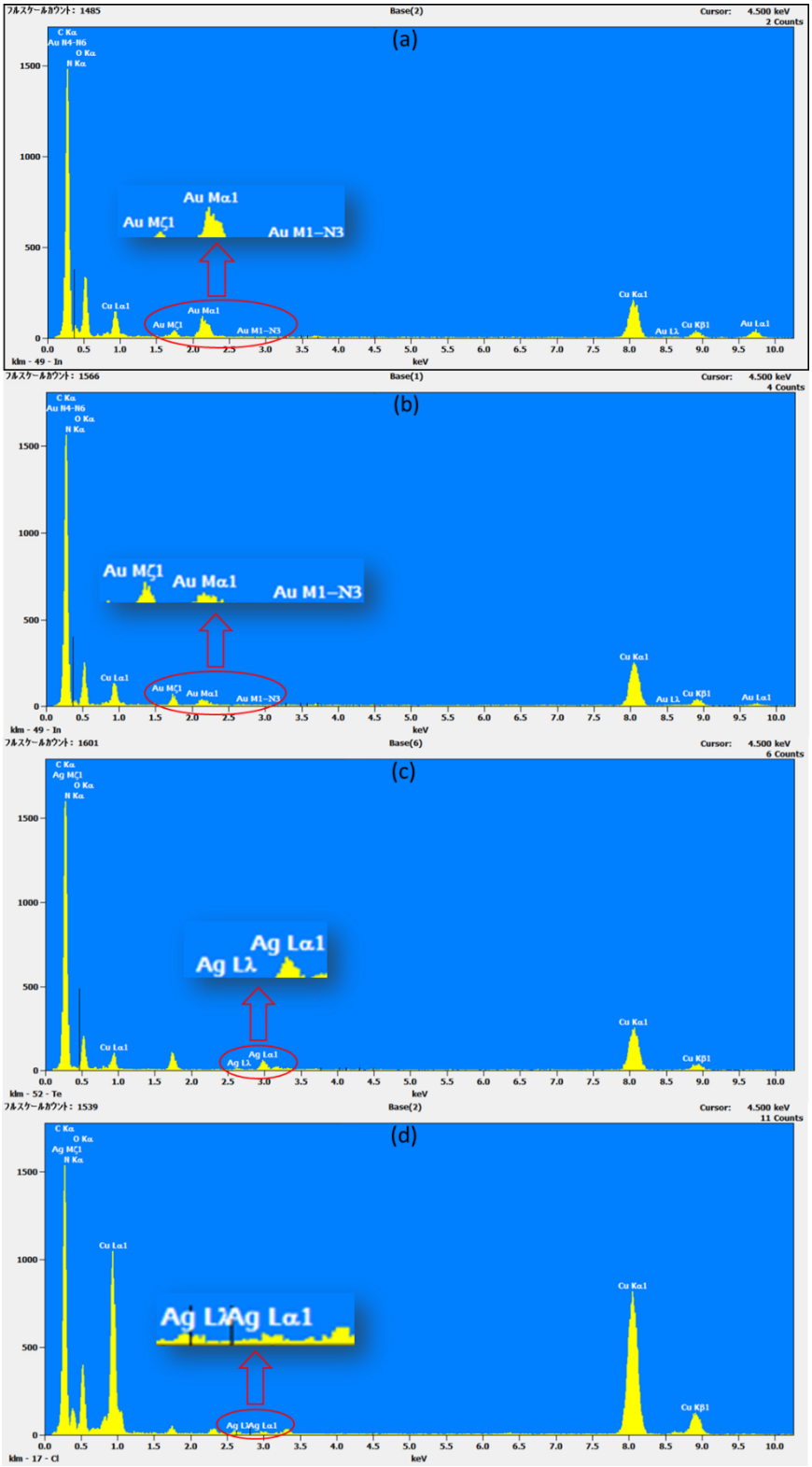

Figure 7. EDS spectra of AuNPs fabricated with (a) and without (b) an ultrasonic field, and AgNPs fabricated with (c) and without (d) an ultrasonic field.

differences between the spectra. Gold was the major component element relative to the others, having been generated from the gold plate. The peaks corresponding to

copper and carbon may originate from the copper grid that was utilized to load the sample. The oxygen and nitrogen elements might originate from contaminants dissolved in the distilled water in the LAL process. These results were the same for the fabricated AgNPs, with no difference between the conditions with and without the ultrasonic field.

Table 1. Zeta potential of colloidal AuNP solution and AgNP solution synthesized by LAL in distilled water in the presence (w/) and absence (w/o) of an ultrasonic field for different ablation times.

Zeta Potential (mV)	10 min w/	10 min w/o	20 min w/	20 min w/o	40 min w/	40 min w/o
Au NPs	**-34.1**	**-30.4**	**-25.6**	**-18.8**	**-24.2**	**-20.5**
Ag NPs	**-36.3**	**-31.2**	**-34.9**	**-30.1**	**-33.0**	**-14.3**

Zeta potential analysis is a technique for determining the surface charge of nanoparticles in colloidal solution and has values that typically range from +100 mV to -100 mV. The magnitude of the zeta potential is predictive of colloidal stability. **Table 1** provides the measurement results of the zeta potential of the fabricated AuNP and AgNP solution. Of note in this table is the fact that the zeta potential of the nanoparticles fabricated by ultrasonic-assisted PLA is higher than that of the nanoparticles synthesized without ultrasound, which means ultrasound could improve the stability of the colloidal solution. An implication of this is the possibility that ultrasound could help to generate more separated nanoparticles and decrease the likelihood of aggregation due to inter-particle attractions. This would result in higher electric potential and degree of stability of the colloidal solution. Moreover, some

researchers [28, 29] have found that the decrease in fabricated nanoparticle size also causes a decrease in zeta potential due to a charge-dependent mechanism in the growth process of the nanoparticles. Such general trend can be observed in our results, given in **Table 3**.

The influence of nanosecond laser pulses on the surface morphology and crater formation of the pure silver plate was investigated under different ablation times (10, 20, and 40 min), and the difference in craters between the situations with and without the ultrasonic field was also examined. **Fig. 8** shows the morphology of the craters analyzed by SEM. It is apparent from these graphs that the craters produced in the presence of the ultrasonic field have shallower depth but more extensive surface area than the craters formed in the absence of the field. Notably, in the case with the ultrasonic field under 20 min ablation time, there are some small bulges on the crater surfaces that increase the roughness of the texture. However, the concentration of the colloidal nanoparticle solution is difficult to measure, yet this is critical for the accurate application of the fabricated nanoparticle solution. Here we provide a novel method to predict the concentration by calculating the volume of the craters on the silver plate ablated by the pulsed laser. The craters on the silver plate were analyzed by laser microscope to obtain fluorescence images containing the crater data. The color values in the fluorescence images were converted to 3D data, which were then extruded to a 3D model and used to calculate the volume of craters by utilizing the image-processing tool and function in MATLAB. **Table 2** shows the calculation results of crater volume, AgNPs concentration in the colloidal solution, UV peak

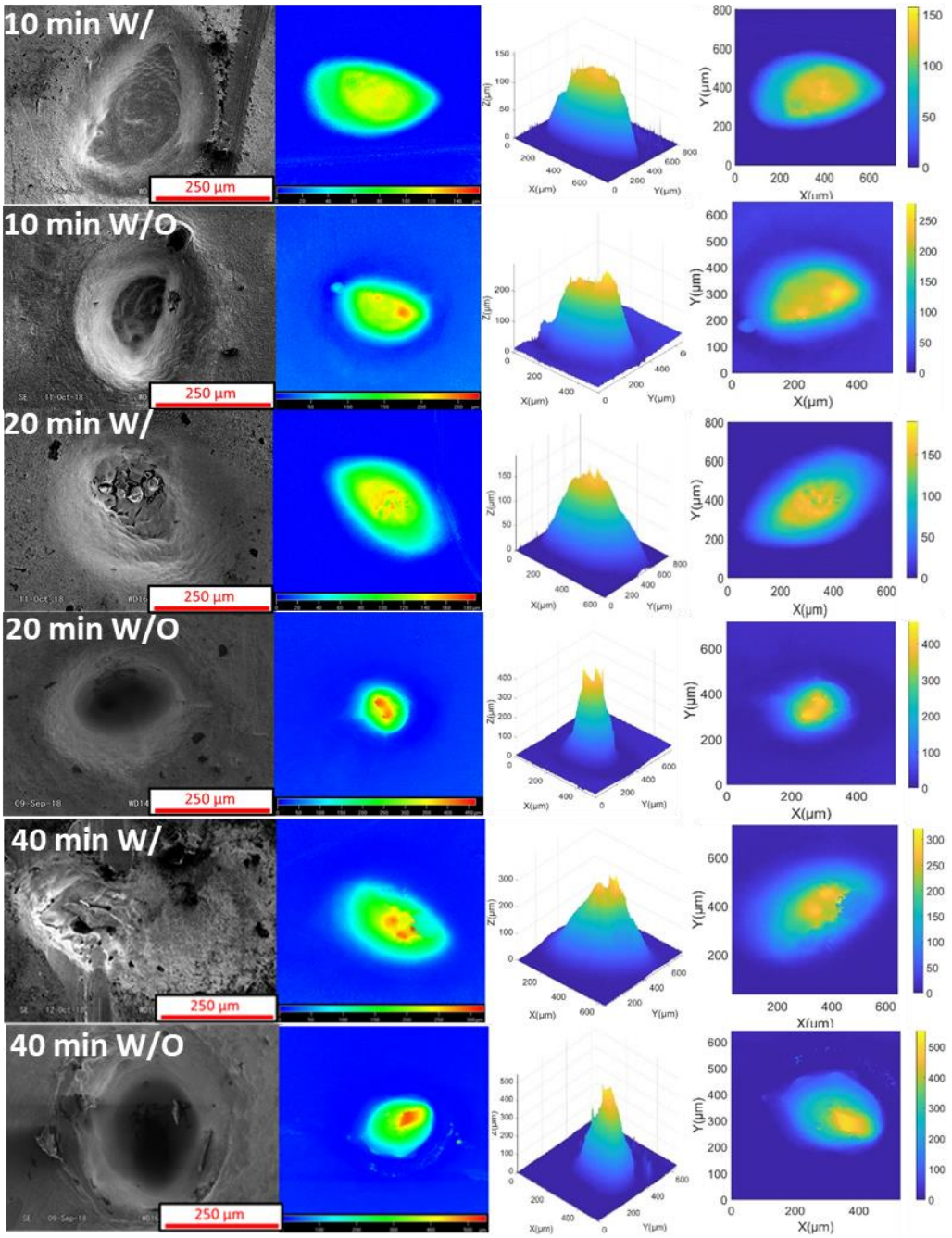

Figure 8. SEM, laser microscope, and simulated MATLAB results of craters on silver plates in the presence (w/) and absence (w/o) of an ultrasonic field for different ablation times.

absorbance, and mass loss per pulse (the amount of silver material removed by a single laser pulse). When the ablation time is 20 min, the volume of the crate in the presence of ultrasonic energy is almost triple than the crater fabricated without ultrasonic field. It is obvious from this table that the craters fabricated in the presence of an ultrasonic field are shallower but have larger volume than those in the situation

without the ultrasonic field for the same ablation time. A possible explanation for this might be that the presence of the ultrasonic field creates several small bubbles in the liquid, which increases the deviation of the irradiation direction of the laser. The ultrasonic-assisted PLA could fabricate craters that are shallower but have more extensive surface area than the typical ablation. Moreover, from **Table 2**, we can see that the mass loss per pulse decreased with ablation time. This result is likely to be related to the absorption of the laser by the nanoparticles on the irradiation path. With the extension of ablation time, the increase in nanoparticles around the plate surface resulted in a decrease in laser energy, which led to a decrease in mass ablation per pulse [30]. This can also be seen from the UV peak absorbance. In the presence of the ultrasonic field, the peak value of absorbance changed from 0.25 to 0.33 as the ablation time increased from 10 to 20 min. However, the peak value changed from 0.33 to 0.37 as the ablation time increased by a further 20 min. The phenomena are the same for the case in the absence of the ultrasonic field.

Table 2. MATLAB and calculation results of craters on silver plates in the presence (w/) and absence (w/o) of an ultrasonic field for different ablation times.

Parameters	Maximal Depth (μm)	Volume (μm^3)	Concentration (ppm)	UV Peak Absorbance (a.u.)	Per Pulse of Mass Loss (g)
10 min w/	157.3	1.31×10^{7}	6.89	0.25	2.28×10^{-8}
10 min w/o	278.3	1.01×10^{7}	5.32	0.16	1.77×10^{-8}
20 min w/	187.6	1.72×10^{7}	9.07	0.34	1.51×10^{-8}
20 min w/o	465.9	1.21×10^{7}	6.41	0.19	1.06×10^{-8}
40 min w/	321.9	2.01×10^{7}	10.56	0.39	8.79×10^{-9}
40 min w/o	548.9	1.39×10^{7}	7.36	0.25	6.08×10^{-9}

Optical emission spectra were observed to study the characteristics of the plasma

plume. **Fig. 9** shows the optical emission spectra of the LAL in the process of ablating the silver plate in distilled water with and without an ultrasonic field, when the laser power was 26.3 J cm^{-2} and the distance between the target and probe was about 6 mm. The spectra caused by different atomic and ionic species in the plume during the ablation process were recorded in the range of 200–1100 nm. Sharp emission lines of Ag atoms and ions were obtained. There is a strong and broad peak in the approximate range of 450–650 nm due to the utilization of a high-power Q-switched pulsed Nd:YAG laser with a wavelength of 532 nm. It is apparent that ultrasound significantly enhanced the plasma emission. A possible explanation for this might be that ultrasound could increase the temperature of the plasma plume and electrons, resulting in an increase in intensity [31].

Table 3. Peak wavelength (WL), absorbance (Abs.), average size (Ave. size), and zeta potential (ζ pot.) results of fabricated AuNPs and AgNPs in the presence and absence of an ultrasonic field for different ablation times.

Gold nanoparticles

Ablation Time	With ultrasonic field				Without ultrasonic field			
	WL (nm)	Abs.	Ave. size (nm)	ζ pot. (mV)	WL (nm)	Abs.	Ave. size (nm)	ζ pot. (mV)
10 min	519	0.15	7.8	-34.1	521	0.14	13.2	-30.4
20 min	518	0.33	5.7	-25.6	521	0.19	9.4	-18.8
40 min	517	0.37	5.4	-24.2	519	0.23	8.3	-20.5

Silver nanoparticles

Ablation Time	With ultrasonic field				Without ultrasonic field			
	WL (nm)	Abs.	Ave. size (nm)	ζ pot. (mV)	WL (nm)	Abs.	Ave. size (nm)	ζ pot. (mV)
10 min	405	0.25	12.1	-36.3	406	0.16	16.8	-31.2
20 min	403	0.34	10.1	-34.9	404	0.19	11.1	-30.1
40 min	403	0.39	7.9	-33.0	407	0.25	10.4	-14.3

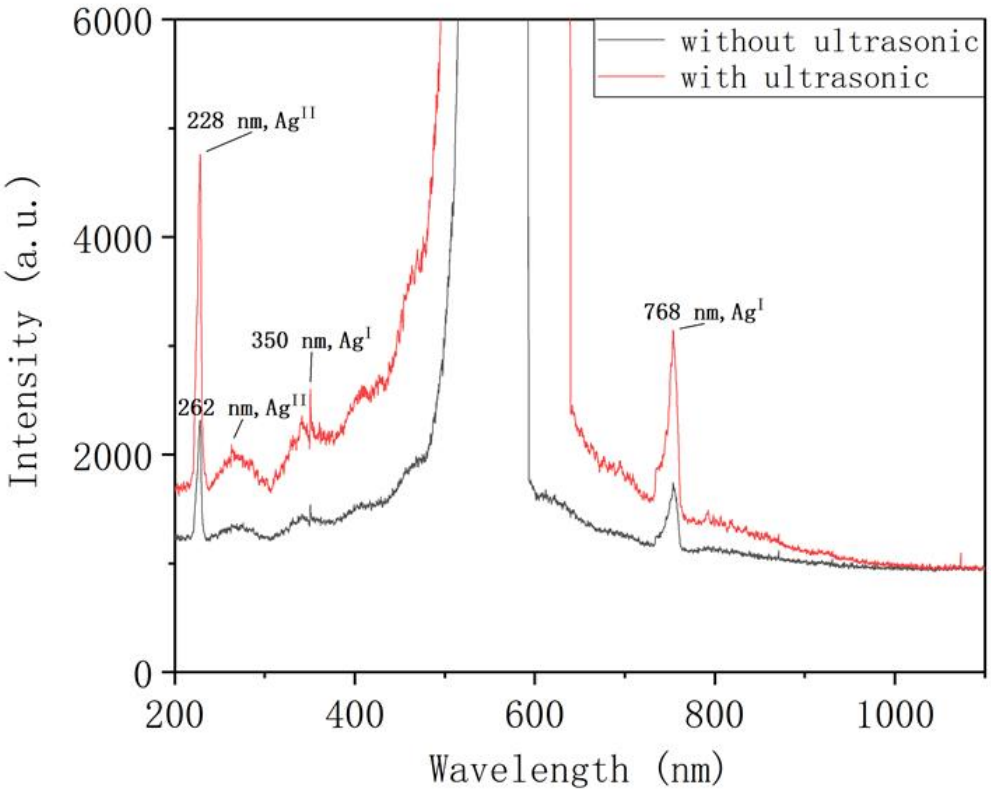

Figure 9. Optical emission spectra for the plasma plume generated in distilled water with and without an ultrasonic field when the laser energy is 26.3 J cm^{-2}.

2-4 Conclusions

AuNPs and AgNPs were fabricated by LAL in distilled water in both the presence and absence of an ultrasonic field. After pure gold and silver plates were ablated by a pulsed Nd:YAG laser, a colloidal nanoparticle solution was obtained. UV–vis spectroscopy analysis showed that ultrasound could enhance the formation rate of nanoparticles in the LAL process. TEM revealed that ultrasound could help to fabricate smaller and more separated metal nanoparticles. Electron diffraction patterns and EDS spectra showed that the AuNPs and AgNPs were both synthesized with and without an ultrasonic field, and there were no obvious differences between the

nanoparticles fabricated in the two different situations. Zeta potential results revealed that ultrasound could improve the stability of the colloidal nanoparticle solution. The peak wavelength (WL), absorbance (Abs.), average size (Ave. size), and zeta potential (ζ pot.) results of fabricated AuNPs and AgNPs in the presence and absence of an ultrasonic field under different ablation times are summarized in **Table 3**. The craters on the silver plates were analyzed by SEM, laser microscope, and MATLAB. The results showed that ultrasound could generate shallower but larger craters due to the generation of small bubbles in the presence of the ultrasonic field. Optical emission results revealed that ultrasound significantly enhanced plasma emission because it could increase the temperature of the plasma plume, resulting in an increase in intensity. The presence of the ultrasonic field in the process of LAL has considerable potential to improve the properties of fabricated metal nanoparticles. These benefits include decreasing the size, preventing aggregation of the nanoparticles, and improving the stability of the nanoparticle suspension.

Reference

[1] A. Khan, R. Rashid, G. Murtaza, A. Zahra, Gold nanoparticles: synthesis and applications in drug delivery, Tropical Journal of Pharmaceutical Research 13(7) (2014) 1169-1177.

[2] Y.-C. Yeh, B. Creran, V.M. Rotello, Gold nanoparticles: preparation, properties, and applications in bionanotechnology, Nanoscale 4(6) (2012) 1871-1880.

[3] N. Elahi, M. Kamali, M.H. Baghersad, Recent biomedical applications of gold nanoparticles: A review, Talanta 184 (2018) 537-556.

[4] K.M.A. El-Nour, A.a. Eftaiha, A. Al-Warthan, R.A. Ammar, Synthesis and applications of silver nanoparticles, Arabian journal of chemistry 3(3) (2010) 135-140.

[5] C. Ziegler, A. Eychmüller, Seeded growth synthesis of uniform gold nanoparticles with diameters of 15− 300 nm, The Journal of Physical Chemistry C 115(11) (2011) 4502-4506.

[6] A.A. Ashkarran, A novel method for synthesis of colloidal silver nanoparticles by arc discharge in liquid, Current Applied Physics 10(6) (2010) 1442-1447.

[7] G. Yang, Laser ablation in liquids: principles and applications in the preparation of nanomaterials, CRC Press2012.

[8] G.W. Yang, Laser ablation in liquids: Applications in the synthesis of nanocrystals, Progress in Materials Science 52(4) (2007) 648-698.

[9] M. Ashokkumar, The characterization of acoustic cavitation bubbles–an overview, Ultrasonics sonochemistry 18(4) (2011) 864-872.

[10] N. TAKAHASHI, T. KUGIMIYA, T. SEKI, K. TERAO, T. KUNOH, M. MIZUNO, Application of ultrasonic cavitation to metal working and surface treatment of mild steel: solid-mechanics, strength of materials, JSME international journal 30(266) (1987) 1229-1236.

[11] N. Takada, A. Fujikawa, N. Koshizaki, K. Sasaki, Effect of ultrasonic

wave on the syntheses of Au and ZnO nanoparticles by laser ablation in water, Applied Physics A 110(4) (2013) 835-839.

[12] D. Barceló, M. de la Guardia, S. Armenta, S. Armenta, M. de la Guardia, Comprehensive Analytical Chemistry, Boston2007.

[13] N.N. Long, C.D. Kiem, S.C. Doanh, C.T. Nguyet, P.T. Hang, N.D. Thien, L.M. Quynh, Synthesis and optical properties of colloidal gold nanoparticles, Journal of Physics: Conference Series, IOP Publishing, 2009, p. 012026.

[14] A.J. Frank, N. Cathcart, K.E. Maly, V. Kitaev, Synthesis of silver nanoprisms with variable size and investigation of their optical properties: a first-year undergraduate experiment exploring plasmonic nanoparticles, Journal of Chemical Education 87(10) (2010) 1098-1101.

[15] Z. Liu, B.X. Wu, A. Samanta, N.G. Shen, H.T. Ding, R. Xu, K.J. Zhao, Ultrasound-assisted water-confined laser micromachining (UWLM) of metals: Experimental study and time-resolved observation, J. Mater. Process. Technol. 245 (2017) 259-269.

[16] T. Nakamura, Y. Herbani, D. Ursescu, R. Banici, R.V. Dabu, S. Sato, Spectroscopic study of gold nanoparticle formation through high intensity laser irradiation of solution, AIP Advances 3(8) (2013) 082101.

[17] H. Guo, C. Ma, L. Thistle, M. Huynh, C. Yu, D. Clasby, B. Chefetz, T. Polubesova, J.C. White, L. He, Transformation of Ag ions into Ag nanoparticle-loaded AgCl microcubes in the plant root zone, Environmental Science: Nano 6(4) (2019) 1099-1110.

[18] M. Raffi, F. Hussain, T. Bhatti, J. Akhter, A. Hameed, M. Hasan, Antibacterial characterization of silver nanoparticles against E. coli ATCC-15224, Journal of materials science and technology 24(2) (2008) 192-196.

[19] J.-S. Park, J.-H. Yoon, H.-J. Kim, Y.-D. Huh, S.-W. Yoon, Laser-induced formation and disintegration of gold nanopeanuts and nanowires, Bulletin of the Korean Chemical Society 31(4) (2010) 819-824.

[20] F. Mafuné, J.-y. Kohno, Y. Takeda, T. Kondow, Formation of gold nanonetworks and small gold nanoparticles by irradiation of intense pulsed laser onto gold nanoparticles, The Journal of Physical Chemistry B 107(46) (2003) 12589-12596.

[21] H. Zeng, X.W. Du, S.C. Singh, S.A. Kulinich, S. Yang, J. He, W. Cai, Nanomaterials via laser ablation/irradiation in liquid: a review, Advanced Functional Materials 22(7) (2012) 1333-1353.

[22] O.R. Musaev, E.A. Sutter, J.M. Wrobel, M.B. Kruger, Au, Ge, and AuGe nanoparticles fabricated by laser ablation, Journal of Nanoparticle Research 14(2) (2012) 654.

[23] H. Feng, G.V. Barbosa-Cánovas, J. Weiss, Ultrasound technologies for food and bioprocessing, Springer2011.

[24] A. Baladi, R.S. Mamoory, Effect of laser wavelength and ablation time on pulsed laser ablation synthesis of Al nanoparticles in ethanol, International Journal of Modern Physics: Conference Series, World Scientific, 2012, pp. 58-65.

[25] S.A. Aromal, V. Vidhu, D. Philip, Green synthesis of well-dispersed gold nanoparticles using Macrotyloma uniflorum, Spectrochimica Acta Part A: Molecular and Biomolecular Spectroscopy 85(1) (2012) 99-104.

[26] C. Liang, K. Zhong, M. Liu, L. Jiang, S. Liu, D. Xing, H. Li, Y. Na, W. Zhao, Y. Tong, Synthesis of morphology-controlled silver nanostructures by electrodeposition, Nano-Micro Letters 2(1) (2010) 6-10.

[27] G. Zhang, J.B. Jasinski, J.L. Howell, D. Patel, D.P. Stephens, A.M. Gobin, Tunability and stability of gold nanoparticles obtained from chloroauric acid and sodium thiosulfate reaction, Nanoscale research letters 7(1) (2012) 337.

[28] D. Riabinina, J. Zhang, M. Chaker, J. Margot, D. Ma, Size control of gold nanoparticles synthesized by laser ablation in liquid media, ISRN Nanotechnology 2012 (2012).

[29] S. Agnihotri, S. Mukherji, S. Mukherji, Size-controlled silver nanoparticles synthesized over the range 5–100 nm using the same protocol and their antibacterial efficacy, Rsc Advances 4(8) (2014) 3974-3983.

[30] H. Desarkar, P. Kumbhakar, A. Mitra, Effect of ablation time and laser fluence on the optical properties of copper nano colloids prepared by laser ablation technique, Applied Nanoscience 2(3) (2012) 285-291.

[31] S. Dadras, P. Jafarkhani, M.J. Torkamany, J. Sabbaghzadeh, Effects of ultrasound radiation on the synthesis of laser ablated gold nanoparticles, Journal of Physics D: Applied Physics 42(2) (2008) 025405.

CHAPTER 3

Synthesis of Hollow PVP/Ag Nanoparticle Composite Fibers via Electrospinning Under a Dense CO_2 Environment

3-1 Introduction

Silver nanoparticles (Ag NPs) have been used in a wide variety of applications, such as biochemical sensing [1], antibacterial coatings [2], and catalysis [3], because of their unique physicochemical properties, which differ from those of their bulk counterparts. They have been synthesized through numerous methods, such as photochemical methods [4], laser ablation [5], chemical reduction [6], and electrochemical techniques [7]. However, most of these synthesis routes produce low yields of Ag NPs and often require the use of hazardous organic solvents, which pose significant environmental and biological risks.

Sonochemical methods have been utilized for the fabrication of nanomaterials, especially noble material NPs, such as Au [8], Ag [9], and Pt [10]. Recent studies report the use of organic molecules under ultrasonic irradiation due to their comparably excellent reductive capability and fair interaction with the particles, which prevents their oxidation and agglomeration [11]. Starch has been identified as an effective surfactant for the fabrication of Ag NPs in some processes because of its biocompatibility and nontoxicity. Kumar et al. [12] successfully synthesized Ag NPs using starch under ultrasonic irradiation. The formation of spherical Ag NPs using

sago starch as a coating agent has also been reported [13].

Electrospinning is a facile technology for fabricating micro- and nanosized polymeric fibers. It has attracted considerable research attention because of its capacity to produce fibers at a large scale. In a conventional electrospinning device, a high-voltage electric area is created between a grounded collector and a spinneret. A syringe pump then feeds the polymer solution via a spinneret into the high-voltage electric area. Hence, the electrostatic force created, rather than the mechanical force, drives the electrospinning process. The synthesized fibers exhibit high surface area-to-volume ratios, which make them suitable as nanoparticle carriers in tissue engineering [14] and controlled-release applications [15] and as electronic sensors [16]. Currently, there has been considerable advancement in the possible applications of hollow fibers in medical applications [17], for gas separation technologies [18], and even in catalysis [19]. Hollow fibers are commonly produced through coaxial capillary or template-assisted methods, where the hollow structure is created through the thermal degradation or selective dissolution of the fiber core. We have reported the fabrication of hollow, nano- and microfibers through simple depressurization under sub- and supercritical CO_2. In contrast, hollow PVP fibers have been successfully synthesized through a facile, one-step electrospinning process under a dense CO_2 environment [20]. Therein, PVP was added to a dichloromethane (DCM) solvent. Subcritical and supercritical CO_2 acts as a poor solvent for virtual polymers [21] and can solubilize most organic solvents, including acids, alcohols, and DCM. Therefore, the interaction between the DCM solution and the dense CO_2 environment

caused the generation and growth of the CO_2-rich voids during the electrospinning process, thereby forming hollow PVP fibers.

In this study, a novel method for producing hollow PVP/Ag NP composite fibers was reported. Ag NPs were synthesized under ultrasonic irradiation using starch as a stabilizing agent. Then, the produced Ag NPs were added to PVP-DCM, which was the precursor solution for the synthesis of the hollow nano- and microfibers. The properties of PVP, such as high solubility in water and organic solvents, low toxicity, excellent film-forming capabilities, and good binding characteristics, make them suitable for the electrospinning process. The characteristics of the products were investigated. Ag NPs imparted antibacterial properties to the electrospun PVP fibers, making the hollow PVP/Ag NPs composite fibers ideal for biomedical applications [22]. The electrospun PVP fibers have high surface area-to-volume ratios because of their hollow morphology. As a result, more Ag NPs were exposed on the surface, thereby enhancing the antibacterial characteristics of the composite fibers [23].

3-2 Experimental Procedures

3-2-1 Materials

A silver nitrate solution ($AgNO_3$, Wako Pure Chemical Industries, Osaka, Japan) was used as the raw material for the ultrasonic process. The starch and distilled water used herein were procured from the same supplier. For the electrospinning process, PVP (MW 1,300,000) (Sigma-Aldrich, Tokyo, Japan) was the solute in the feed solution, whereas DCM (99.0% purity, Wako Pure Chemical Industries) was used as

the solvent. Lastly, carbon dioxide (CO_2, 99% purity) was purchased from Sogo Kariya Sanso, Inc., Kariya, Japan.

3-2-2 Synthesis and Characterization of Ag NPs

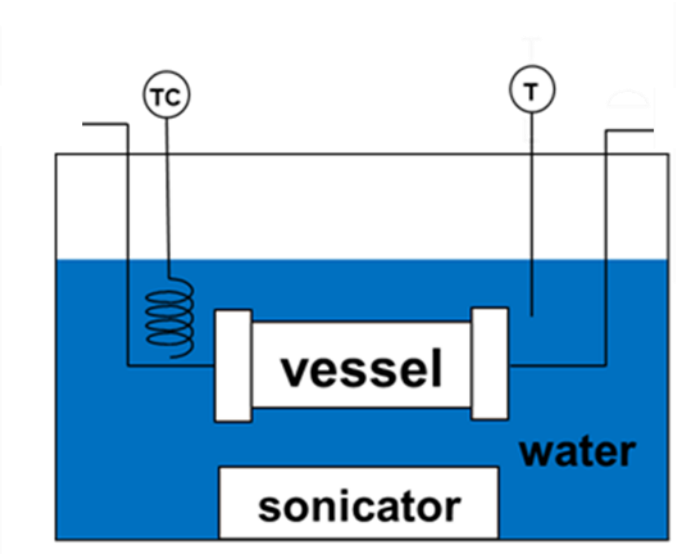

Figure 1. Ultrasonic irradiation apparatus for the synthesis of Ag NPs

Starch (10 mg) was added to a 10 mL-10 mM $AgNO_3$ solution in a glass bottle. To ensure full dissolution of the surfactant, the mixture was stirred and then agitated ultrasonically. The solution was then placed in a water bath maintained at 50 °C. Ultrasonic irradiation was carried out using Ultrasonic Multi Cleaner W–118 (Honda Electronics Company, Toyohashi, Japan). Irradiation was done at 28, 45, 100 kHz, and 600 W (input) for 40, 80, and 120 min. **Fig. 1** shows the schematic of the ultrasonic irradiation apparatus. The optical characteristics of the Ag NPs colloidal solution were investigated using ultraviolet-visible (UV-vis) spectrometry (V-550, JASCO Corporation, Tokyo, Japan). To investigate the morphology and elemental spectra of the produced Ag NPs, transmission electron microscopy (TEM, JEM-

2100Plus, JEOL, Tokyo, Japan) with energy-dispersive X-ray spectroscopy (EDX, JED-2300T & Gatan, GIF Quantum ER, JEOL) was done. For such analysis, the Ag NP colloidal solution was dipped onto a TEM grid. From the obtained TEM images, the size distribution of the synthesized Ag NPs was analyzed using ImageJ ver. 1.42, at least 250 nanoparticles were counted for analysis.

3-2-3 Feed Solution Preparation for Electrospinning

The polymer solution was produced by dissolving 6, 8, and 10 wt% PVP in DCM. Then, a 1 mL Ag NP solution was added to the polymer solution. Prior to this addition, the colloidal Ag NPs solution was freeze-dried using FDU-1200 (EYELA, Tokyo Rikakikai Co, Ltd., Tokyo, Japan).

3-2-4 Synthesis of the Hollow PVP and PVP/Ag NPs Composite Fibers

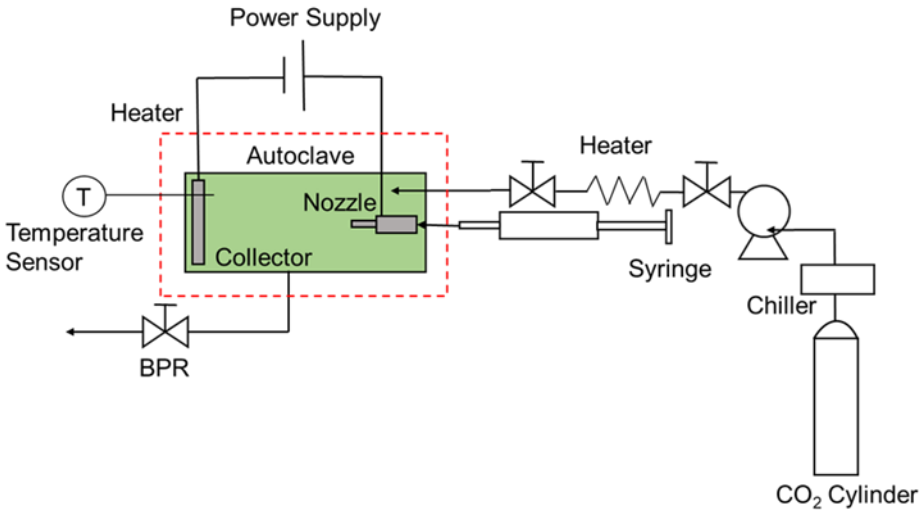

Figure 2. Schematic representation of the electrospinning system.

Fig. 2 shows the apparatus used for the electrospinning process, which included a

non–conductive PEEK chamber (AKICO, Tokyo, Japan) with cartridge heaters coupled with an electric fan, high-pressure pump (PU–1586, JASCO), back–pressure regulator (BPR) (HPB–450 SUS–316, AKICO), high-pressure syringe pump (PHD–Ultra 4400, Harvard Apparatus, Massachusetts, US), a high-voltage (HV) power supply unit (HARb–30P1, Matsusada Precision Inc., Tokyo, Japan), and an 8 mL stainless-steel syringe. The nozzle-to-collector distance was 8 cm. The PEEK chamber was heated to 314 ± 3 K. The temperature of the electrospinning process was regulated using a thermocouple, which was installed inside and was put in direct contact with the space of the PEEK vessel. In contrast, K-type thermocouples were installed on the vessel walls to monitor the radial temperature distribution in the PEEK chamber. After the desired temperature was reached, CO_2 was pumped into the vessel using a PEEK capillary tube to the desired pressure, which was maintained using a BPR. As the necessary conditions were achieved, the polymer feed solution was injected by the high-pressure syringe pump into the chamber through the capillary tube at a flow rate of 0.05 mL/min. Simultaneously, an electrostatic force was generated at 15 kV using the HV power supply. In this device, the polymer solution and CO_2 were moved separately using a nozzle and were then placed in the stainless-steel flange (anodic electrode). Each experiment was carried out for 20 min and was repeated two to four times to obtain reliable results.

3-2-5 Characterization of the Hollow PVP and PVP/Ag NPs Composite Fibers

The morphology of the produced fibers was examined using SEM (S-4300,

Hitachi, Tokyo, Japan) after gold coating (IB-3, Eiko Engineering, Tokyo, Japan). The gold coating was approximately 10 nm thick. ImageJ version 1.42 software was used to determine fiber diameter from the SEM images. And the number of the fibers counted for analysis was at least 300. The functional groups on the surfaces of the electrospun fibers generated under each experimental condition were identified through FT-IR spectroscopy (Spectrum Two FT-IR spectrophotometer, PerkinElmer Ltd., Waltham, US) in the attenuated total reflectance (ATR) mode (golden single reflection ATR system, P/N 10500 series, Specac) at 4 cm^{-1} resolution from 4000–500 cm^{-1}. The structures of the fibers were investigated using X-ray diffraction (XRD; FR–E X-ray diffractometer with Cu Kα radiation (λ = 1.542 Å)). The beam size was approximately 300 μm × 300 μm, whereas the camera length was approximately 70 mm. The fiber samples were placed on a glass substrate and treated with an X-ray beam without additional modifications. The thermal behavior of the electrospun fibers was evaluated using thermogravimetric/differential thermal analyses (TG 8120; Thermo plus, Rigaku, Corp., Tokyo, Japan). Surface elemental compositions of the products were studied using XPS (ESCA-3300, Shimadzu-Kratos, Kyoto, Japan) at a collecting angle of 45° from the average.

3-3 Results and discussion

3-3-1 Fabrication and Characterization of the Ag NPs Synthesized by Ultrasonic Irradiation

The unique optical properties of Ag NPs, that is, the localized surface plasmon

resonance (LSPR), are dependent on their shape, diameter, surface structure, and aggregation state, and make them ideal materials for various applications. **Fig. 3** shows the UV spectra of the Ag NP solutions fabricated through ultrasonic irradiation at different frequencies and sonication durations. An intense peak at the spectra of the Ag NP solution occurs approximately at 405 nm, which was also observed in the spectra of chemically prepared Ag NPs reported in literature [24]. **Fig. 3a** shows the optical absorbance of the colloidal Ag NP solutions obtained at different ultrasonic frequencies (28, 45, and 100 kHz) and irradiation for 40 min. The color of the Ag NP solution changed from transparent (100 kHz) to yellow (45 kHz), and finally, to dark brown (28 kHz), which indicates a change in the rate of reduction of $AgNO_3$ to Ag NPs [25]. The absorbance of the Ag NP solution decreased as the ultrasonic frequency increased. Furthermore, the intensity of the peak at 405 nm decreased with increasing ultrasonic frequency, which implies that the formation rate of Ag NPs in the colloidal solution decreased with increasing frequency [26]. Previous reports tell that the following reactions occur during the sonochemical reduction of metal nanoparticles in the presence of organic additives (reactions 1—4) [27].

$$H_2O \rightarrow {}^{\bullet}H + {}^{\bullet}OH \quad (1)$$

$$2RH + {}^{\bullet}OH({}^{\bullet}H) \rightarrow 2\,{}^{\bullet}R + H_2O(H_2) \quad (2)$$

$$RH \rightarrow \text{radicals and unsteady products} \quad (3)$$

$$Ag(I) + \text{reducing species } ({}^{\bullet}H, {}^{\bullet}R, \text{etc.}) \rightarrow Ag(0) \quad (4)$$

where RH is the organic additive. Reactions (1)–(3) demonstrate the sonochemical fabrication of the reducing radicals and reductants: (1) the sonolysis of water produces

•H, (2) the abstraction reaction of RH with •OH or •H produces •R and H_2, and (3) the pyrolysis of RH and water produces radicals and unsteady compounds. Finally, Ag(I) reduction occurs through many complex reaction steps utilizing the produced reducing species in the previous reactions [28]. Low sonication frequencies can create relatively large bubbles that collapse more forcefully than higher frequencies, thus promoting the generation of more reducing radicals and reductants. Furthermore, low frequencies can motivate collisions between molecules and clusters in the solution, thereby accelerating the reduction of $AgNO_3$ to form Ag NPs.

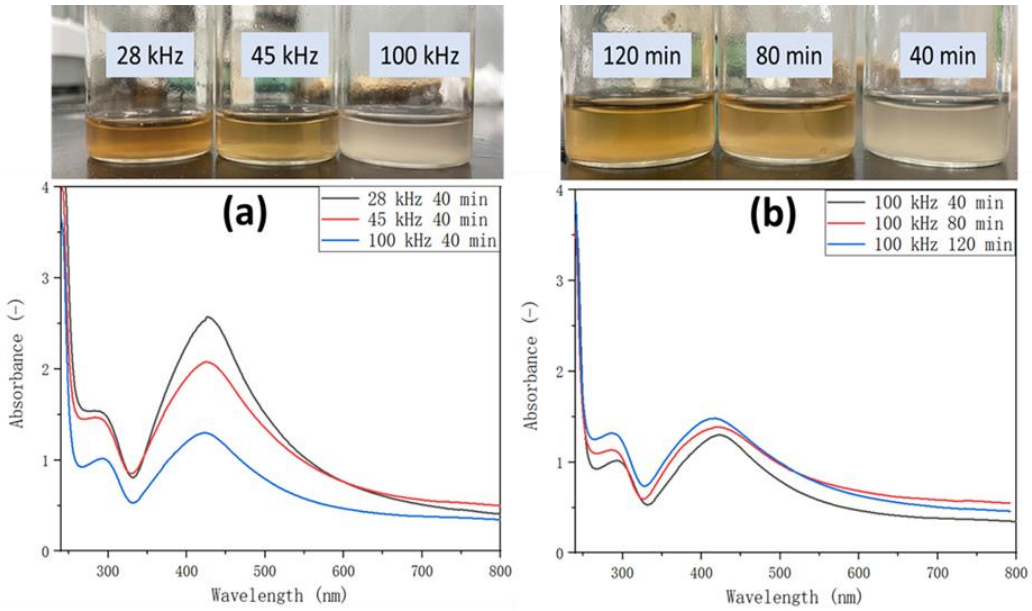

Figure 3. (a) UV spectra of the colloidal Ag NP solutions produced through ultrasonic irradiation at different frequencies (28, 45, and 100 kHz) for 40 min sonication duration, and (b) different ultrasonic times (40, 80, and 120 min) at frequency of 100 kHz.

Fig. 3b shows the UV spectra of the Ag NP solutions obtained at different ultrasonic times (40, 80, and 120 min) at a frequency of 100 kHz. The nanoparticle

solution was transparent after ultrasonication for 40 min. Its color turned yellow after 80 min and darkened after 120 min. The observed transition in the color is possibly due to the change in the Ag NP concentration in the solution with varying ultrasonication durations. Furthermore, the absorbance of the solution increased with increasing ultrasonic time, which corresponds well to the previous conclusion. Longer ultrasonication times imply more time for the reduction of $AgNO_3$ to Ag NPs; hence, increasing Ag NP concentration was observed with prolonged sonication. In addition, the LSPR band shifted toward a shorter wavelength area (**Fig. 3a, b**), when the ultrasonic frequency and the sonication time were increased. This shift indicates a reduction in the Ag NP particle size. The mechanism of such phenomenon will be discussed in the next section.

Fig. 4 shows the TEM images, the selected area electron diffraction (SAED) graphs and size distribution of the Ag NPs fabricated at different ultrasonic irradiation frequencies and times. The synthesized Ag NPs are dispersed and have spheroidal morphologies. The observed diffuse bands in the SAED patterns can be indexed to the (111), (200), (220), and (311) diffraction planes of Ag, which helps determine the phase of the NPs [29]. No discernible differences were observed on changing the ultrasonic parameters, indicating that the frequency and ultrasonic time had no major effect on the crystallinity of the produced Ag NPs. However, ultrasonic parameters were found to have a considerable effect on the size of the nanoparticles. Smaller nanoparticles, by definition, exhibit greater surface area-to-volume ratios, resulting in superior properties. For instance, smaller Ag NPs were reported to have better

antibacterial characteristics [30]. The particle size distribution plots show that the size of the fabricated Ag NPs decreased with increasing frequency (**Fig. 4a-c**) and ultrasonic time (**Fig. 4c-e**). Ultrasonic irradiation of the solution generates transient cavitation: bubble formation, growth, and implosive collapse. When a bubble bursts, it creates intense shock waves that spread faster than the speed of sound through the liquid, causing unique sonochemical reactions and high-velocity collisions among the solid particles suspended in the liquid [31]. At 28 kHz ultrasonic frequency, high

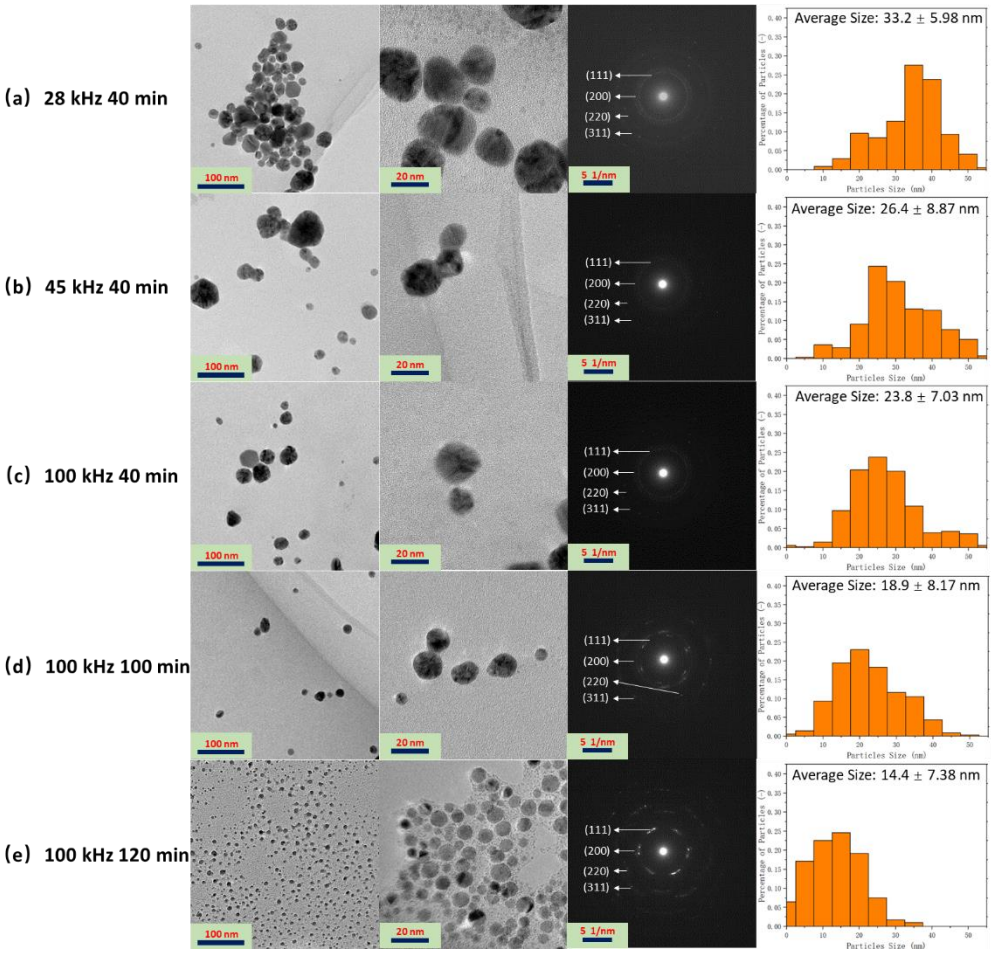

Figure 4. TEM images and SAED patterns of Ag NPs fabricated at different ultrasonic irradiation frequencies (28, 45, and 100 kHz) and durations (40, 80, and 120 min).

collisions occurred among the Ag NPs, which resulted in the fusion of the nanoparticles, atoms, or electrons formed from localized melting. This phenomenon can be alleviated at 45 and 100 kHz frequency, hence the decreasing Ag NPs size with increasing ultrasonic frequencies. The findings of this study are in good agreement with those of previous reports. Suslick et al. [32] reported that metal particles that have a mean size of 5–10 μm were aggregated by ultrasonic irradiation at 20 kHz. Okitsu et al. [27] also generated Au NPs using sonochemical reduction of Au (III) ions and found that nanoparticle size decreased with higher ultrasonic frequency during sonication at 20–213 kHz frequencies. In case of ultrasonic time, longer ultrasonic times prevented the aggregation of the NPs, thus reducing the size of the

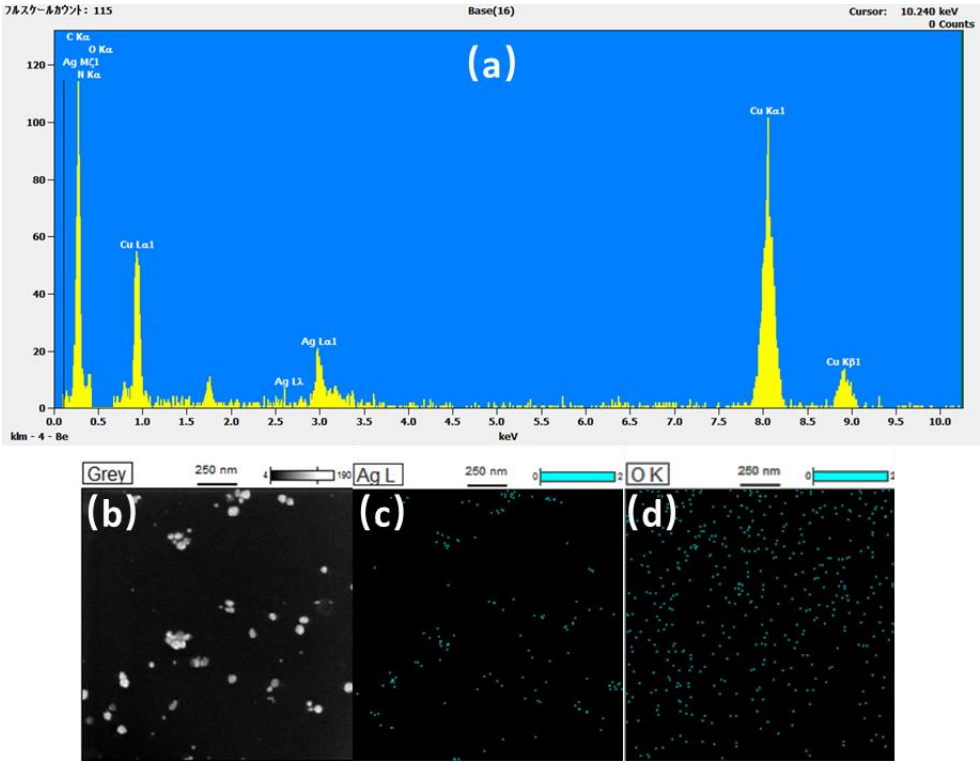

Figure 5. EDX spectra (a) and dark-field TEM image of Ag NPs (b) with the corresponding EDX map for silver (c) and oxygen (d) (ultrasonic frequency: 100 kHz, ultrasonic time: 120 min).

synthesized Ag NPs. A similar finding was reported in the synthesis of zinc oxide NPs through sonication [33].

Elemental characterization was carried out using EDX analysis. **Fig. 5a** shows the EDX spectra of the Ag NPs synthesized at 100 kHz with sonication for 120 min. Strong signals relating to the elemental silver region (3 keV) in the EDX spectrum, indicates the formation of Ag NPs in the solution products. Peaks corresponding to silver, copper (Cu), carbon (C), oxygen (O), and nitrogen (Ni) were also observed in the EDX spectra. The Cu and C peaks observed may be attributed to the TEM grid utilized to load the Ag NPs. In contrast, the peaks corresponding to O and N are attributed to the starch molecule attached to the surface of the Ag NPs and from the $AgNO_3$ solution, respectively.

3-3-2 Fabrication and Characterization of Electrospun PVP Fibers

Fig. 6 shows the SEM images of the PVP fibers synthesized with and without dense CO_2 at an applied voltage of 15 kV using different concentrations (6, 8, and 10 wt%) of the PVP-DCM solution. Without dense CO_2, that is, under atmospheric conditions, and at a low polymer solution concentration (6 wt%), the electrospun products showed irregular morphologies and blend (**Fig. 6a**). Furthermore, at the same PVP concentration, almost no solidified electrospun product could be found on the electrospinning collector. The viscosity varies directly with the concentration of polymer, which, in turn, considerably influences the electrohydrodynamic process. Low viscosity can cause the surface tension of the PVP polymer solution to become high. Additionally, incomplete evaporation of the solvent during the electrospinning

process occurred when a non-viscous polymer mixture was used as the starting solution, thereby causing the formation of non-solidified, wet electrospun products [34]. In contrast, spherical PVP particles and nascent strings were produced when an 8 wt% PVP polymer solution was utilized (**Fig. 6c**). The increase in the PVP concentration possibly reduced the surface tension and increased the viscosity of the PVP-DCM solution. At 10 wt% PVP, wet fibers were formed on the collector, as seen in **Fig. 6e**.

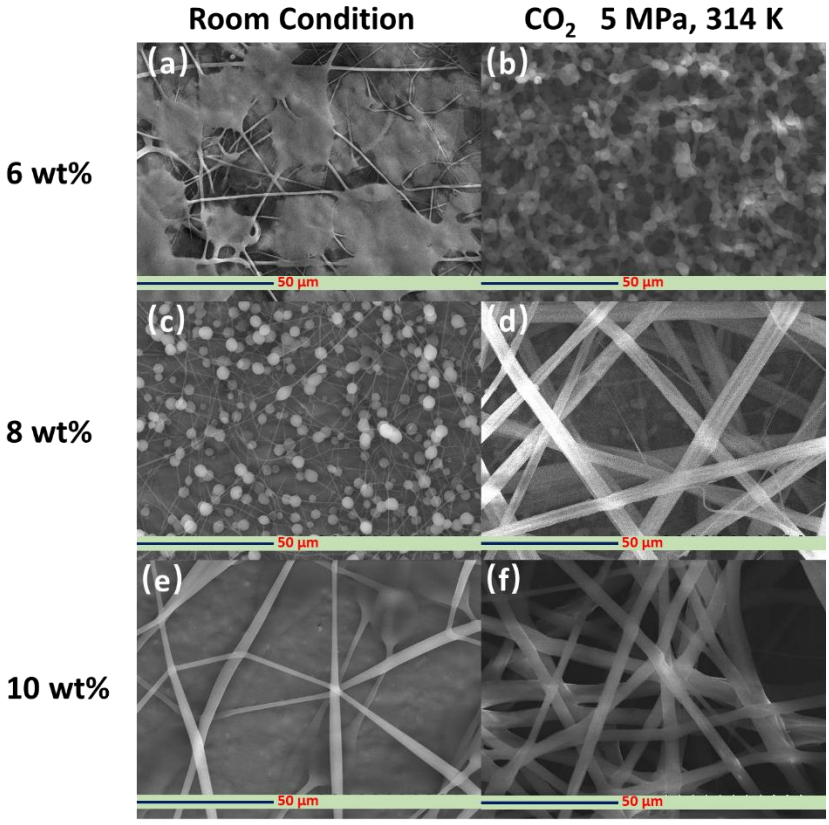

Figure 6. SEM images of the PVP fibers fabricated with (b, d, f) and without (a, c, e) dense CO_2 at 15 kV at different PVP concentrations (6, 8, 10 wt%).

Under dense CO_2 environment (pressure: 5 MPa, temperature: 314 K), the electrospun products formed using the 6 wt% PVP solution were mostly nano- and

micro-sized spherical particles (**Fig. 6b**). Additionally, almost no PVP polymer strings were synthesized under such operating conditions. Majority of the PVP particles had shriveled morphologies with uniform sizes. These findings imply the rapid evaporation of the solvent, DCM, which resulted to the shrinkage of the PVP particles. By increasing the PVP concentration from 6 to 8 wt% in the presence of dense CO_2, smooth PVP polymer fibers with nonuniform sizes were fabricated (**Fig. 6d**). These suggest that by changing the PVP concentration and consequently, the surface tension of the PVP-DCM polymer solution, the morphologies of the electrospun products can be controlled from the accompanied tuning of the evaporation rate of the solvent. A further increase in the PVP concentration to 10 wt% led to the fabrication of smooth, bead-free fibers (**Fig. 6f**). The fibers were straight and appeared to have flat (ribbon-like) morphologies. In addition, the size was more uniform than that of the products fabricated from 8 wt% PVP-DCM solution. Similar results were obtained when the concentration of the PVP solution was changed during the electrospinning process in [35]. The results herein imply that when the concentration of the PVP feeding solution was increased, the entanglement of the PVP chains increased, which promoted the initiation and formation of smooth and uniform-sized electrospun fibers under ambient temperature and a dense CO_2 environment. Thus, a 10 wt% PVP solution was chosen as the feed solution for the subsequent electrospinning experiments under dense CO_2.

Fig. 7 shows the SEM images of the PVP fibers fabricated using a 10 wt% PVP polymer solution with and without dense CO_2 at different applied voltages (12, 15,

and 18 kV). The applied voltage can determine the intensity of the generated electrical field during the electrospinning process, which significantly affects the characteristics of the PVP solution jet that produces the electrospun fibers. Therefore, the applied voltage is critical for determining the morphology of the electrospun fibers [36]. At higher applied voltages, the stretching stress on the solution jet typically increases, resulting in more delicate fibers. The generation of defects along the fibers is also promoted, increasing the likelihood of bead formation when using an inadequate concentration of the polymer feeding solution [37]. Under room conditions, wet fibers were successfully fabricated under all applied voltage conditions (**Fig. 7a, c, e**). However, under dense CO_2 conditions, significant differences emerged. As shown in

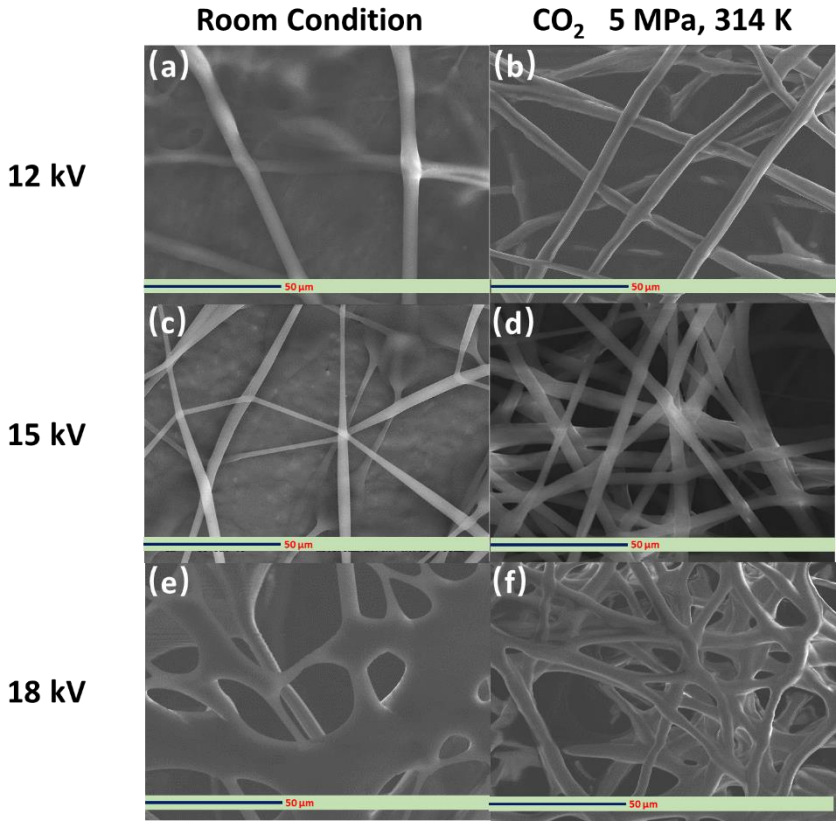

Figure 7. SEM images of PVP fibers fabricated from 10 wt% PVP solution with (b, d, f) and without (a, c, e) dense CO_2 at various applied voltage (12, 15, 18 kV).

Fig. 7b, the fibers fabricated at an applied voltage of 12 kV were not straight. Defects along the fiber direction were also visible. These may be caused by the angle of PVP molecules in the long electrospinning process. At an applied voltage of 18 kV, the electrospun fibers appear to be slightly wet and not straight (**Fig. 7f**), which is possibly caused by the low evaporation rate of DCM as a consequence of shorter electrospinning duration. Olive et al. [38] studied the effect of applied voltage on electrospun fibers and found similar results. Furthermore, the results show that a 15 kV applied voltage was suitable to fabricate the electric field in the electrospinning process (**Fig. 7d**).

3-3-3 Fabrication and Characterization of the Hollow PVP/Ag NP Composite Fibers

Atmospheric parameters, such as temperature and relative humidity, may also impact the morphology of the electrospun fibers in addition to the characteristics of the polymer solution and the factors affecting the electrohydrodynamic process. **Fig. 8** shows the SEM images of the hollow PVP/Ag NP composite fibers fabricated using the 10 wt% PVP solution under various CO_2 pressures (room conditions, 1, 3, and 5 MPa) at an applied voltage of 15 kV. Under room conditions, the electrospun products mainly consisted of wet fibers (**Fig. 8a**). At a 1 MPa-CO_2 pressure, the products are composed solely of nano-and microparticles. No PVP strings are formed (**Fig. 8b**). After increasing the operating pressure to 3 MPa, spherical particles with PVP strings were formed (**Fig. 8c**). At 5 MPa, the products exhibited a uniform, fine fiber morphology (**Fig. 8d**). Bead formation was not observed, which was in agreement

with the results of Huang et al. [39]. The average diameter of the electrospun fibers was approximately 5.02 ± 1.87 μm. From the cross-sectional image in **Fig. 8e**, the hollow structure of the fibers can be seen. The formation mechanism of such hollow fibers is as follows. First, the interaction between the polymer solution containing the Ag NPs and CO_2 may accelerate the rapid evaporation of the solvent (DCM). The phase boundaries then emerge, and eventually, the electrospun fiber PVP products. Even under supercritical conditions, CO_2 is an extremely poor solvent for most polymers (including DCM) under the same conditions [40]. As such, superfluous CO_2 can dissolve into the DCM-rich liquid phase of the PVP polymer solution with Ag NPs. Subsequently, the spinodal decomposition of the PVP-DCM solution might

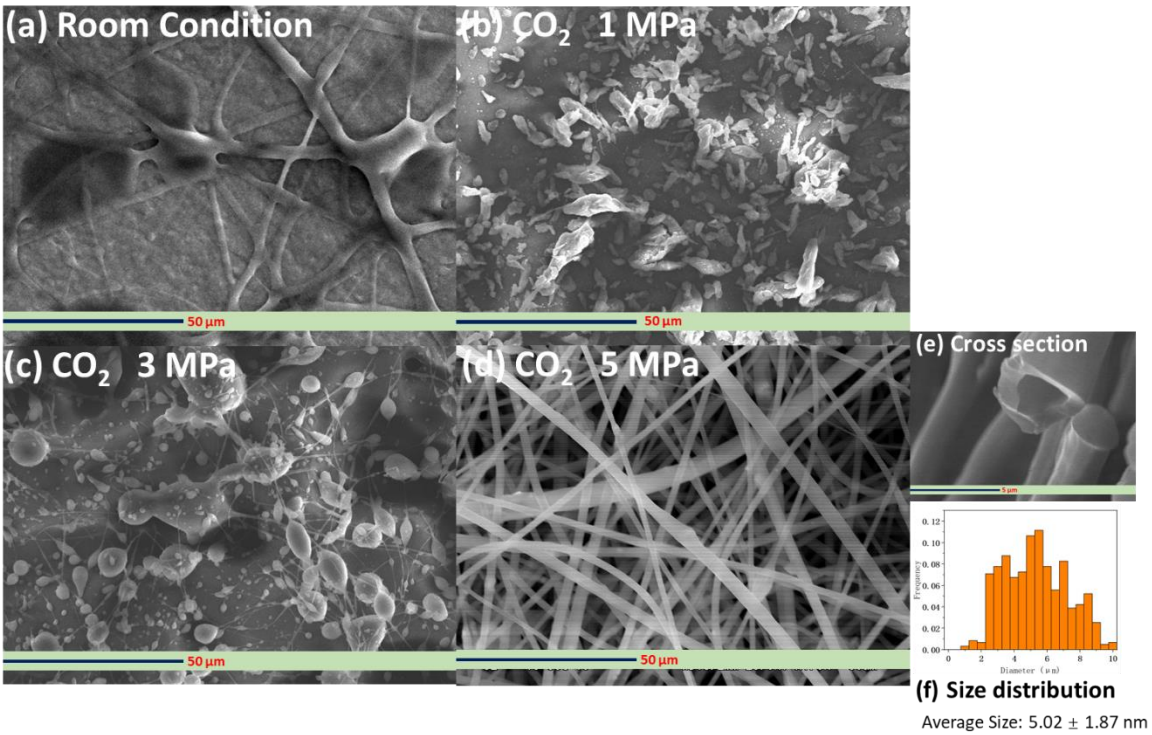

Figure 8. SEM images of the hollow PVP fibers fabricated from PVP solution containing Ag NPs under various CO_2 conditions (room conditions, and 1, 3, 5 MPa).

occur, resulting to the generation of a PVP-DCM solution network containing CO_2-rich bubbles. Such bubbles in the polymer solution might coalesce and expand, forming a jet against the PVP-rich network and propelling PVP-rich phase bubbles radially outward against the inner surface of the jet. This explains the hollow-core-morphology of the electrospun PVP fibers containing Ag NPs [41]. Wahyudiono et al. [42] also reported that hollow PVP fibers containing titanium dioxide (TiO_2) particles were formed using PVP-DCM containing TiO_2 NP solution by electrospinning under dense CO_2. In that report, TiO_2 NPs were directly added to the PVP-DCM solution. However, because of the low solubility of TiO_2 in the DCM solution, aggregation between the nanoparticles was observed, resulting to the no dispersion of the particles on the surface of the fibers and the formation of micro-sized clusters in some areas.

Fig. 9 shows the FT-IR spectra of the pure PVP fibers and of the PVP/Ag NP composite fibers electrospun at 5 MPa and an applied voltage of 15 kV. The peak positions of the infrared bands and functional groups are summarized in **Table 1** [42].

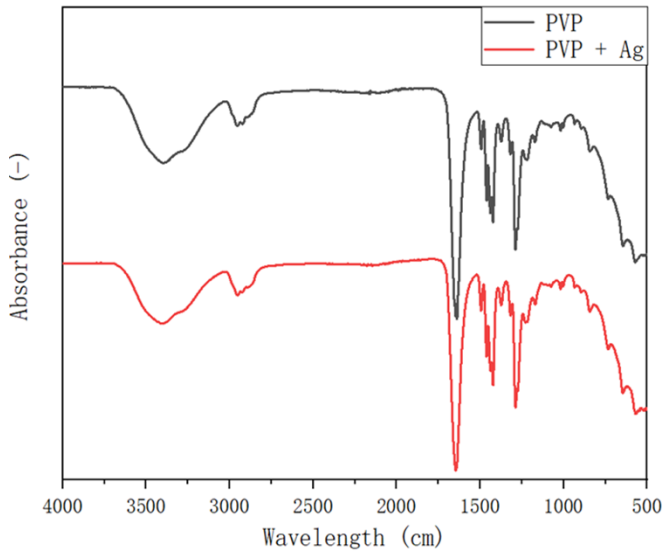

Figure 9. FT-IR spectrum of the pure PVP fibers and of the PVP/Ag NP composite fibers electrospun at 5 MPa and applied voltage of 15 kV.

Herein, FT-IR spectra were used to analyze the possible structural changes in the PVP molecule, as well as the interaction between PVP and Ag NPs. The synthesized PVP/Ag NP composite fibers share the same FT-IR spectral properties with PVP, suggesting that the products fabricated by electrospinning had almost the same functional groups. Furthermore, this finding suggests that only a small amount of Ag NPs is present in the composite fibers. Hotaby et al. [43] also found a similar result by comparing the FT-IR spectra of pure PVP and PVP-Ag nanocomposite films.

Table 1. Typical bands in infrared spectra of PVP.

Wavenumber (cm^{-1})	**Functional groups**
3435.47-3415.45 and 1286.37-1284.84	N–H stretching vibration and C–N stretching vibration from pyrrolidone structure
2950.02-2921.18	C–H stretching for aliphatic compounds
1651.12-1650.46	Carbonyl (C–O) stretching of the five-membered cyclic lactam structure
1493.25-1493.16 and 1461.00-1460.82	C=C aromatic stretching
1422.11-1421.63 and 1372.91-1372.32	C–H bending vibration from methylene groups (aliphatic compound)
843.82-843.29	=C–H bending vibrations (unsaturated compounds)

Fig. 10 shows the XRD patterns of the pure PVP fibers and of the PVP/Ag NP composite fibers electrospun at 5 MPa at an applied voltage of 15 kV. Two diffused halo peaks close to $2\theta = 11.78°$ and 21.94° were observed in the XRD pattern of the pure PVP fiber. This is in good agreement with the results reported by Li et al. [44]. In

contrast, the XRD pattern of the PVP/Ag NP composite fibers showed peaks at 2θ = 11.47° and 21.63°. These results also point out the meager amount of Ag NPs in the synthesized PVP/Ag NP composite. These findings may also be due to the masking of

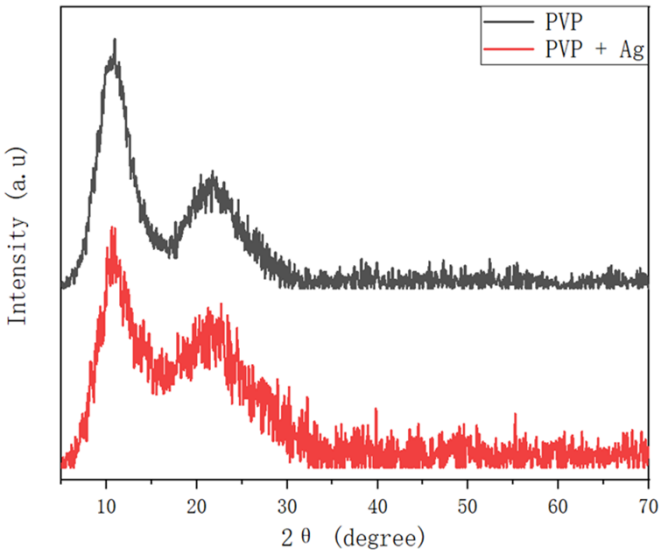

Figure 10. XRD pattern of the pure PVP fibers and of the PVP/Ag NP composite fibers electrospun at 5 MPa at an applied voltage of 15 kV.

the peaks corresponding to Ag NPs by the PVP fibers [43].

Fig. 11 shows the TGA curves of the pure PVP fibers and of the PVP/Ag NP composite fibers (synthesized at 5 MPa and an applied voltage of 15 kV). By measuring the weight variations in response to rising temperature at a constant heating rate, TGA may evaluate a material's thermal stability and the proportion of the volatile component. Heat transfer and medium diffusion may be used to explain this phenomenon [45]. In this experiment, TGA was carried out at an airflow of 100 mL min^{-1} and a heating rate of 10 °C min^{-1}. Pure PVP and electrospun PVP fibers containing Ag NPs were weighed (about 0.6–1 mg) in aluminum pans. After that, the

weight loss of these two groups was monitored during the heating process from 40 to 800 °C. The thermal degradation of the pure PVP fibers and of the PVP/Ag NP composite fibers was considered to be the reason for the weight loss observed in **Fig. 11**. During the TG analysis, several sections of loss were observed. The initial weight loss observed at 80 °C is possibly due to the evolution of the volatile compounds from pure PVP and electrospun PVP/Ag NP composite fibers. Thereafter, the thermal deterioration of the electrospun products began at approximately 270 °C. This was followed by a considerable weight loss until 630 °C from the primary devolatilization of the fibers. No further change in weight was observed for both samples beyond this temperature. In general, the polymer matrix–nanoparticle structure can enhance the thermal stability [46]. During the rapid evaporation of DCM, Ag NPs may be dispersed into the PVP matrix. Then, a powerful interaction between PVP and Ag NPs forms through hydrogen bonding in the PVP matrix. Nevertheless, as can be seen in

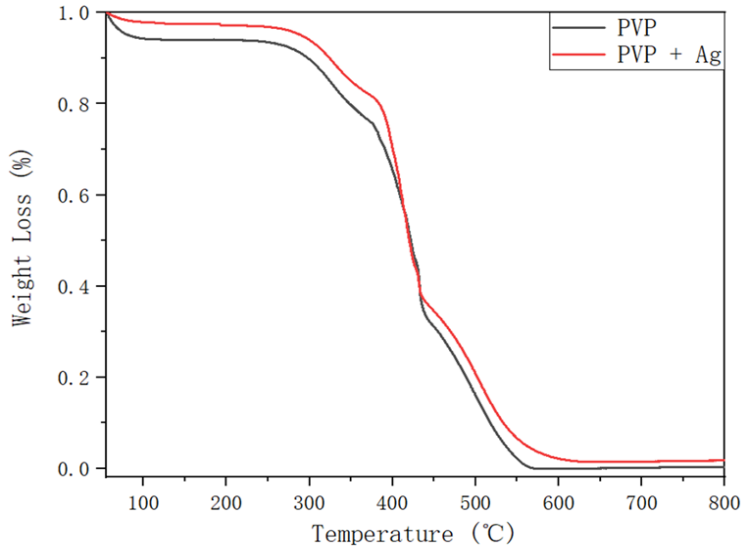

Figure 11. TGA curves of the pure PVP fibers and of the PVP/Ag NP composite fibers electrospun at 5 MPa and applied voltage of 15 kV.

Fig. 11, there were no significant differences in the thermal degradation curves of the pure PVP and of the PVP/Ag NP composite fibers possibly due to the low amount of Ag NPs added to the PVP-DCM solution. Consequently, the thermal stability of the PVP/Ag NP composite fibers may not be considerably modified.

The residue weight (0.025 mg) observed the TG curve of PVP/Ag NP composite fibers (0.73 mg) at temperatures beyond 630 °C reveal the existence of Ag NPs in the electrospun PVP fibers (**Fig. 11**). This permits the separation of the nanoparticles from the polymer, allowing for XPS examination of the sample to acquire precise information on the chemical state of the metal. XPS examination was used after TGA to verify the presence of Ag NPs in the residue. **Fig. 12** shows the XPS spectra of the residue obtained after the TG analysis of the PVP/Ag NP fibers (5 MPa dense CO_2 and an applied voltage of 15 kV). Peaks were detected at 368 and 374 eV in the spectra, indicating the presence of Ag NPs in the residue after the TG analysis [47].

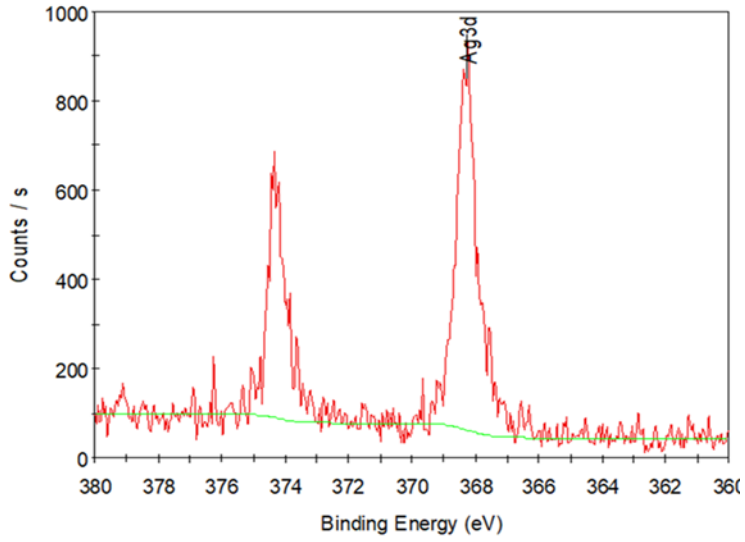

Figure 12. XPS spectra of the residue obtained after the TG analysis of the PVP/Ag NP fibers (5 MPa and applied voltage of 15 kV).

3-4 Conclusions

In this study, Ag NPs were initially synthesized through ultrasonic irradiation using starch as a stabilizing and reducing agent of the $AgNO_3$ solution. The sonochemical reduction route has an extraordinary potential for generating Ag NPs with a desirable particle size. The ultrasonic frequency and time were found to have a considerable impact on the morphology of the fabricated Ag NPs. In addition, electrospinning of PVP fibers with different PVP concentrations (6, 8, and 10 wt%) at 12–18 kV was investigated under room conditions and dense CO_2 environment (temperature: 313 K, pressure: 5 MPa). The electrospinning products were compared using SEM images, and suitable parameters for the synthesis of hollow PVP fibers were determined. Thereafter, the electrospinning of PVP-Ag NP fibers was studied at different CO pressures. SEM images revealed that the electrospun PVP/Ag NP composite fibers exhibited the same morphology and hollow structure as the pure PVP fibers. FT-IR spectroscopy and XRD analysis revealed that the pure PVP fibers and PVP/Ag NP composite fibers exhibited similar properties. In addition, XPS confirmed the presence of Ag NPs in the residue obtained after the TG analysis of the hollow PVP/Ag NP composite. Thus, the results showed that polymer fibers with hollow structures containing metal NPs can be fabricated by electrospinning under dense CO_2.

Reference

[1] K. Shrivas, N. Nirmalkar, M.K. Deb, K. Dewangan, J. Nirmalkar, S. Kumar,

Application of functionalized silver nanoparticles as a biochemical sensor for selective detection of lysozyme protein in milk sample, Spectrochimica Acta Part A: Molecular and Biomolecular Spectroscopy 213 (2019) 127-133.

[2] G. Franci, A. Falanga, S. Galdiero, L. Palomba, M. Rai, G. Morelli, M. Galdiero, Silver nanoparticles as potential antibacterial agents, Molecules 20(5) (2015) 8856-8874.

[3] R. Chimentao, I. Kirm, F. Medina, X. Rodriguez, Y. Cesteros, P. Salagre, J. Sueiras, Different morphologies of silver nanoparticles as catalysts for the selective oxidation of styrene in the gas phase, Chemical communications (7) (2004) 846-847.

[4] M. Zaarour, M. El Roz, B. Dong, R. Retoux, R. Aad, J. Cardin, C. Dufour, F. Gourbilleau, J.-P. Gilson, S. Mintova, Photochemical preparation of silver nanoparticles supported on zeolite crystals, Langmuir 30(21) (2014) 6250-6256.

[5] X. Hu, N. Takada, S. Machmudah, Wahyudiono, H. Kanda, M. Goto, Ultrasonic-Enhanced Fabrication of Metal Nanoparticles by Laser Ablation in Liquid, Industrial & Engineering Chemistry Research 59(16) (2020) 7512-7519.

[6] H. Wang, X. Qiao, J. Chen, S. Ding, Preparation of silver nanoparticles by chemical reduction method, Colloids and Surfaces A: Physicochemical and Engineering Aspects 256(2-3) (2005) 111-115.

[7] R.A. Khaydarov, R.R. Khaydarov, O. Gapurova, Y. Estrin, T. Scheper, Electrochemical method for the synthesis of silver nanoparticles, Journal of Nanoparticle Research 11(5) (2009) 1193-1200.

[8] W. Chen, W. Cai, L. Zhang, G. Wang, L. Zhang, Sonochemical processes and formation of gold nanoparticles within pores of mesoporous silica, Journal of colloid and interface science 238(2) (2001) 291-295.

[9] M. Darroudi, A.K. Zak, M. Muhamad, N. Huang, M. Hakimi, Green synthesis of colloidal silver nanoparticles by sonochemical method, Materials Letters 66(1) (2012) 117-120.

[10] Y. Mizukoshi, E. Takagi, H. Okuno, R. Oshima, Y. Maeda, Y. Nagata, Preparation of platinum nanoparticles by sonochemical reduction of the Pt (IV) ions: role of surfactants, Ultrasonics sonochemistry 8(1) (2001) 1-6.

[11] H.S. Shin, H.J. Yang, S.B. Kim, M.S. Lee, Mechanism of growth of colloidal silver nanoparticles stabilized by polyvinyl pyrrolidone in γ-irradiated silver nitrate solution, Journal of colloid and interface science 274(1) (2004) 89-94.

[12] B. Kumar, K. Smita, L. Cumbal, A. Debut, R.N. Pathak, Sonochemical synthesis of silver nanoparticles using starch: a comparison, Bioinorganic Chemistry and Applications 2014 (2014).

[13] D.K. Božanić, V. Djoković, J. Blanuša, P. Nair, M. Georges, T. Radhakrishnan, Preparation and properties of nano-sized Ag and Ag 2 S particles in biopolymer matrix, The European Physical Journal E 22(1) (2007) 51-59.

[14] M. Rahmati, D.K. Mills, A.M. Urbanska, M.R. Saeb, J.R. Venugopal, S. Ramakrishna, M. Mozafari, Electrospinning for tissue engineering applications,

Progress in Materials Science 117 (2021) 100721.

[15] G.-M. Kim, A. Wutzler, H.-J. Radusch, G.H. Michler, P. Simon, R.A. Sperling, W.J. Parak, One-dimensional arrangement of gold nanoparticles by electrospinning, Chemistry of materials 17(20) (2005) 4949-4957.

[16] A. Chinnappan, C. Baskar, S. Baskar, G. Ratheesh, S. Ramakrishna, An overview of electrospun nanofibers and their application in energy storage, sensors and wearable/flexible electronics, Journal of Materials Chemistry C 5(48) (2017) 12657-12673.

[17] T.W. Cheung, L. Li, A review of hollow fibers in application-based learning: From textiles to medical, Textile Research Journal 89(3) (2019) 237-253.

[18] E. Lasseuguette, J.-C. Rouch, J.-C. Remigy, Hollow-fiber coating: Application to preparation of composite hollow-fiber membrane for gas separation, Industrial & Engineering Chemistry Research 52(36) (2013) 13146-13158.

[19] X. Ji, Z. Su, P. Wang, G. Ma, S. Zhang, Tethering of nicotinamide adenine dinucleotide inside hollow nanofibers for high-yield synthesis of methanol from carbon dioxide catalyzed by coencapsulated multienzymes, ACS nano 9(4) (2015) 4600-4610.

[20] S. Machmudah, H. Kanda, S. Okubayashi, M. Goto, Formation of PVP hollow fibers by electrospinning in one-step process at sub and supercritical CO2, Chemical Engineering and Processing: Process Intensification 77 (2014)

1-6.

[21] C.F. Kirby, Phase behavior of polymers in supercritical fluid solvents, Chem. Rev. 99 (1999) 565-602.

[22] H.Ç. Vatansever, A.E. Meriçboyu, Production of antibacterial polyvinylpyrrolidone nanofibers containing silver nanoparticles via electrospinning method, MANAS Journal of Engineering 7(1) 13-23.

[23] D.-G. Yu, M.-Y. Teng, W.-L. Chou, M.-C. Yang, Characterization and inhibitory effect of antibacterial PAN-based hollow fiber loaded with silver nitrate, Journal of Membrane Science 225(1-2) (2003) 115-123.

[24] A.J. Frank, N. Cathcart, K.E. Maly, V. Kitaev, Synthesis of silver nanoprisms with variable size and investigation of their optical properties: a first-year undergraduate experiment exploring plasmonic nanoparticles, Journal of Chemical Education 87(10) (2010) 1098-1101.

[25] G. Sharma, J.-S. Nam, A.R. Sharma, S.-S. Lee, Antimicrobial potential of silver nanoparticles synthesized using medicinal herb coptidis rhizome, Molecules 23(9) (2018) 2268.

[26] N. Takada, A. Fujikawa, N. Koshizaki, K. Sasaki, Effect of ultrasonic wave on the syntheses of Au and ZnO nanoparticles by laser ablation in water, Applied Physics A 110(4) (2013) 835-839.

[27] K. Okitsu, M. Ashokkumar, F. Grieser, Sonochemical synthesis of gold nanoparticles: effects of ultrasound frequency, The Journal of Physical Chemistry B 109(44) (2005) 20673-20675.

[28] R. Salkar, P. Jeevanandam, S. Aruna, Y. Koltypin, A. Gedanken, The sonochemical preparation of amorphous silver nanoparticles, Journal of materials chemistry 9(6) (1999) 1333-1335.

[29] G. Zhang, J.B. Jasinski, J.L. Howell, D. Patel, D.P. Stephens, A.M. Gobin, Tunability and stability of gold nanoparticles obtained from chloroauric acid and sodium thiosulfate reaction, Nanoscale research letters 7(1) (2012) 337.

[30] M. Raffi, F. Hussain, T. Bhatti, J. Akhter, A. Hameed, M. Hasan, Antibacterial characterization of silver nanoparticles against E. coli ATCC-15224, Journal of materials science and technology 24(2) (2008) 192-196.

[31] S.J. Doktycz, K.S. Suslick, Interparticle collisions driven by ultrasound, Science 247(4946) (1990) 1067-1069.

[32] T. Prozorov, R. Prozorov, K.S. Suslick, High velocity interparticle collisions driven by ultrasound, Journal of the American Chemical Society 126(43) (2004) 13890-13891.

[33] R. Mahdavi, S.S.A. Talesh, The effect of ultrasonic irradiation on the structure, morphology and photocatalytic performance of ZnO nanoparticles by sol-gel method, Ultrasonics Sonochemistry 39 (2017) 504-510.

[34] A.S. Levitt, R. Vallett, G. Dion, C.L. Schauer, Effect of electrospinning processing variables on polyacrylonitrile nanoyarns, Journal of Applied Polymer Science 135(25) (2018) 46404.

[35] H. Ozawa, S. Machmudah, H. Kanda, M. Goto, Electrospraying technique under pressurized carbon dioxide for hollow particle production, Reactive and

Functional Polymers (2019).

[36] V. Beachley, X. Wen, Effect of electrospinning parameters on the nanofiber diameter and length, Materials Science and Engineering: C 29(3) (2009) 663-668.

[37] Y. Liu, L. Dong, J. Fan, R. Wang, J.Y. Yu, Effect of applied voltage on diameter and morphology of ultrafine fibers in bubble electrospinning, Journal of Applied Polymer Science 120(1) (2011) 592-598.

[38] L. Can-Herrera, A. Oliva, M. Dzul-Cervantes, O. Pacheco-Salazar, J. Cervantes-Uc, Morphological and mechanical properties of electrospun polycaprolactone scaffolds: effect of applied voltage, Polymers 13(4) (2021) 662.

[39] S. Huang, L. Zhou, M.-C. Li, Q. Wu, Y. Kojima, D. Zhou, Preparation and properties of electrospun poly (vinyl pyrrolidone)/cellulose nanocrystal/silver nanoparticle composite fibers, Materials 9(7) (2016) 523.

[40] M.S. Shin, J.H. Lee, H. Kim, Phase behavior of the poly (vinyl pyrrolidone)+ dichloromethane+ supercritical carbon dioxide system, Fluid phase equilibria 272(1-2) (2008) 42-46.

[41] Wahyudiono, K. Okamoto, S. Machmudah, H. Kanda, M. Goto, Hydrophilic polymer composites synthesized by electrospinning under dense carbon dioxide, AIP Conference Proceedings, AIP Publishing, 2015, p. 040010.

[42] H. Ozawa, S. Machmudah, H. Kanda, M. Goto, Electrospinning of poly (vinyl pyrrolidone) fibers containing metal oxide nanoparticles under dense CO

2, Research on Chemical Intermediates 44(4) (2018) 2215-2230.

[43] W. El Hotaby, H. Sherif, B. Hemdan, W. Khalil, S. Khalil, Assessment of in situ-Prepared Polyvinylpyrrolidone-Silver Nanocomposite for Antimicrobial Applications, Acta Physica Polonica, A. 131(6) (2017).

[44] X.-G. Li, I. Kresse, J. Springer, J. Nissen, Y.-L. Yang, Morphology and gas permselectivity of blend membranes of polyvinylpyridine with ethylcellulose, Polymer 42(16) (2001) 6859-6869.

[45] A. Arenillas, F. Rubiera, C. Pevida, J. Pis, A comparison of different methods for predicting coal devolatilisation kinetics, Journal of analytical and applied pyrolysis 58 (2001) 685-701.

[46] K. Chrissafis, D. Bikiaris, Can nanoparticles really enhance thermal stability of polymers? Part I: An overview on thermal decomposition of addition polymers, Thermochimica Acta 523(1-2) (2011) 1-24.

[47] Z. Zhang, X. Zhang, Z. Xin, M. Deng, Y. Wen, Y. Song, Synthesis of monodisperse silver nanoparticles for ink-jet printed flexible electronics, Nanotechnology 22(42) (2011) 425601.

List of Publications

[1] X. Hu, N. Takada, S. Machmudah, Wahyudiono, H. Kanda, M. Goto, Ultrasonic-Enhanced Fabrication of Metal Nanoparticles by Laser Ablation in Liquid, Industrial & Engineering Chemistry Research 59(16) (2020) 7512-7519.

[2] X. Hu, J. He, L. Zhu, S. Machmudah, Wahyudiono, H. Kanda, M. Goto, Synthesis of Hollow PVP/Ag Nanoparticle Composite Fibers via Electrospinning under a Dense CO_2 Environment, Polymers 14(1) (2022) 89.

[3] L. Zhu, Y. Zhu, X. Hu, Y. Lin, S. Machmudah, Wahyudiono, H. Kanda, M. Goto, PVP Electrospun Fiber fabrication with Evenly Dispersed Silver Nanoparticles using Ultrasonic Pre-Nozzle Electrospinning. (Under Review)

Acknowledgments

Throughout the writing of this thesis, I have received a great deal of support and assistance.

I would first like to thank my supervisor, Prof Goto Motonobu whose expertise was invaluable in formulating the research questions and methodology. Your insightful feedback pushed me to sharpen my thinking and brought my work to a higher level.

I would also like to thank to Dr Hideki Kanda, for his valuable guidance throughout my studies. You provided me with the tools that I needed to choose the right direction and successfully complete my dissertation.

In addition, I would like to thank to Dr. Wahyudiono and Dr. Takada Noriharu for their wonderful collaboration and patient support. You are always there for me.

Finally, I could not have completed this dissertation without the support of my friends in Goto lab, who provided stimulating discussions as well as happy distractions to rest my mind outside of my research.